Palaeogeography, Palaeoclimatology, Palaeoecology 518 (2019) 97–118

Contents lists available at ScienceDirect

Palaeogeography, Palaeoclimatology, Palaeoecology

journal homepage: www.elsevier.com/locate/palaeo

Quaternary history of the Lake Magadi Basin, southern Kenya Rift: Tectonic and climatic controls

R. Bernhart Owen[a,*], Robin W. Renaut[b], Veronica M. Muiruri[c], Nathan M. Rabideaux[d], Tim K. Lowenstein[e], Emma P. McNulty[e], Kennie Leet[e], Daniel Deocampo[f], Shangde Luo[g], Alan L. Deino[h], Andrew Cohen[i], Mark J. Sier[j,k], Christopher Campisano[l], Chuan-Chou Shen[m,n], Anne Billingsley[i], Anthony Mbuthia[o], Mona Stockhecke[p]

[a] Department of Geography, Hong Kong Baptist University, Kowloon Tong, Hong Kong
[b] Department of Geological Sciences, University of Saskatchewan, Saskatoon, SK S7N 5E2, Canada
[c] Palynology and Palaeobotany Section, Department of Earth Sciences, National Museums of Kenya, P.O. Box 40658, 00100 Nairobi, Kenya
[d] Department of Chemistry, Rutgers University, Newark, NJ 07102, USA
[e] Department of Geological Sciences, State University of New York, Binghamton, NY 13902, USA
[f] Department of Geosciences, Georgia State University, GA 30302, USA
[g] Department of Earth Sciences, National Cheng-Kung University, 701 Tainan, Taiwan, Republic of China
[h] Berkeley Geochronology Center, Berkeley, CA 94709, USA
[i] Department of Geosciences, University of Arizona, Tucson, AZ 85721, USA
[j] Department of Earth Sciences, University of Oxford, OX1 3AN Oxford, United Kingdom
[k] Centro Nacional de Investigación sobre la Evolución Humana, 09002 Burgos, Spain
[l] Institute of Human Origins, School of Human Evolution and Social Change, Arizona State University, Tempe, AZ 85287-4101, USA
[m] High-Precision Mass Spectrometry and Environment Change Laboratory, Department of Geosciences, National Taiwan University, 10617 Taipei, Taiwan, Republic of China
[n] Research Center for Future Earth, National Taiwan University, 10617 Taipei, Taiwan, Republic of China
[o] Tata Chemicals Magadi, Box 1, Magadi, Kenya
[p] Large Lakes Observatory (LLO), University of Minnesota Duluth, Duluth, MN 55812, USA

ARTICLE INFO

Keywords:
Rift basins
Geochemistry
Sedimentology
Palaeolakes
Diatoms
Mineralogy

ABSTRACT

Sediments from the Magadi Basin (south Kenya Rift) preserve a one-million-year palaeoenvironmental record that reflects interactions between climatic, volcanic and tectonic controls. Climate changes that impacted sedimentation include wet-dry cycles on variable timescales and an overall progressive trend towards greater aridity. Volcanic influences involved inputs of tephra to the basin, significant inflow of geothermal fluids, and the effects of weathering, erosion and transportation of clastics from trachyte and basalt terrains. Tectonic controls, which were often step-like, reflect the influence of faults that provided pathways for fluids and which controlled accommodation space and drainage directions.

Intensified aridity and evaporative concentration resulted in salinity and pH increasing with time, which led to a change from calcite deposition in mildly saline lakes before 380 ka to the later formation of zeolites from reactions of volcaniclastic debris with highly alkaline lake and pore water. After 105 ka, hyperalkaline conditions led to trona accumulation and increasingly variable rare earth elements (REEs). The presence of mixed saline and freshwater diatom taxa between 545 and 16 ka indicates climate variability and episodic inputs of fresh water to saline lakes. Calcrete formed in lake marginal settings during semi-arid periods.

Tectonic controls operated independently of climate, but they interacted together to determine environmental conditions. Aquatic deposition was maintained during periods of increasing aridity because fault-controlled ambient and geothermal springs continued to flow lakewards. This recharge, in turn, limited pedogenesis: palaeosols are common in other rift floor sequences. Trona formed when aridity and evapoconcentration increased, but its precipitation also reflects increased magmatic CO_2 that ascended along faults. Basin fragmentation and north-south fractures caused loss of cross-rift (east-west) drainage from rift-marginal basalts, resulting in reduced transition metals after 545 ka. The Magadi Basin demonstrates how a careful reconstruction of these complex tectono-climatic interactions is essential for accurate palaeoenvironmental reconstruction in continental rifts and in other tectonic settings.

* Corresponding author.
E-mail address: owen@hkbu.edu.hk (R. Bernhart Owen).

https://doi.org/10.1016/j.palaeo.2019.01.017
Received 15 October 2018; Received in revised form 19 December 2018; Accepted 8 January 2019
Available online 14 January 2019
0031-0182/

1. Introduction

Much of the early palaeoclimate research in East Africa was devoted to understanding Plio-Pleistocene hominin and archaeological sites (see Cohen et al., 2016 and Campisano et al., 2017 for reviews). More recently, efforts have focused on climate variability from various Pliocene to Recent time-slices (Kingston et al., 2007; Owen et al., 2008; Tierney et al., 2010; Junginger and Trauth, 2013; Magill et al., 2013). A range of record types have proven useful in reconstructing palaeoclimates in the region, including Late Quaternary core-records (e.g., Verschuren and Chapman, 2008; De Cort et al., 2013, 2018), outcrop data (e.g., Levin, 2015), and marine cores (e.g., deMenocal, 1995, 2004). More recently, drill cores from extant rift lakes have proven exceptionally useful in documenting palaeoenvironmental histories, including a 1.3-million-year Lake Malawi record (Ivory et al., 2016). In addition, a one-million-year pollen-diatom-mineralogy study of a core at Lake Magadi synthesised the regional climatic history for the southern Kenya Rift as a basis for exploring hominin evolution and mammalian change (Owen et al., 2018a). The latter paper complements this study, which is based on outcrops and two lake cores, and which focuses on aquatic sedimentation and palaeoenvironments using sedimentological, mineralogical and geochemical data, supplemented by diatom analyses.

Lake Magadi lies in the axial trough of the southern Kenya Rift ~605 m above sea level (masl), and is a seasonally-flooded, saline

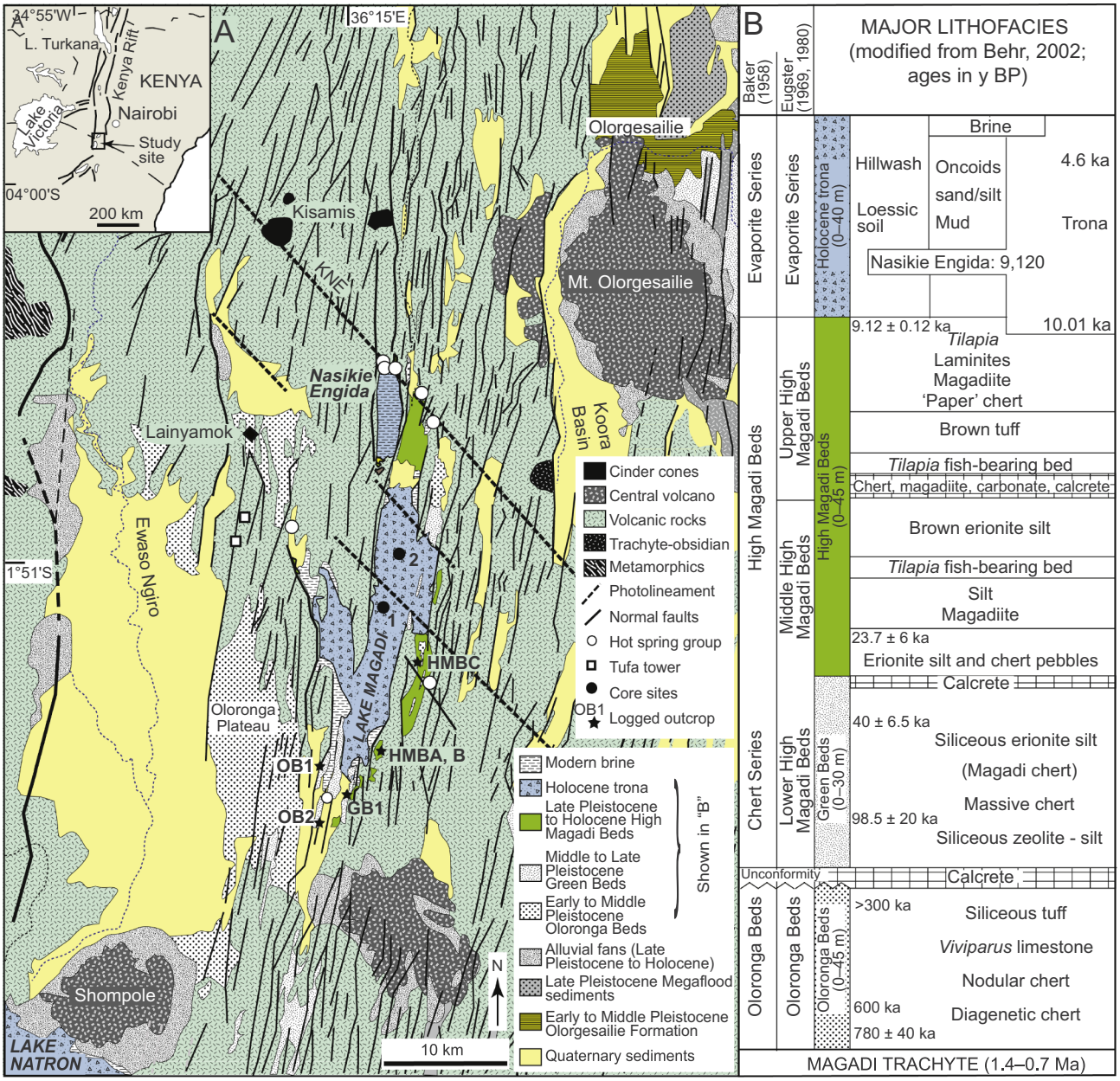

Fig. 1. Geology and stratigraphy of the Magadi Basin, south Kenya Rift. A: Geological setting based on Baker (1958, 1963), Behr (2002), Guth and Wood (2014) and original observations. Photolineaments imply subvolcanic (?) NW–SE trends that have locally controlled the morphology of the Magadi Basin, drainage and alignment of hot-spring groups. Drill Site 1 (MAG14-1A and -1C) lies near the western edge of a structural high with depth to trachyte of ~133 m; drill Site 2 (MAG14-2A) lies within a sub-basin (rhomb-graben?) with depth to trachyte basement of ~194 m. KNE = Kisamis-Nasikie Engida-Koora lineament. Logged outcrops: HMB = High Magadi Beds (localities A, B and C); GB = Green Beds (locality 1); OB = Oloronga Beds (localities 1 and 2). B: Magadi Basin stratigraphy modified from Behr (2002) showing evolving terminology and revisions, with earlier schemes to the left. No thickness or timescale is implied. Four informal units are currently recognised based on outcrops: the Oloronga Beds, the Green Beds, the High Magadi Beds and the Evaporite Series. The stratigraphy and radiometric ages are from Behr (2002). Published dates reported by Behr are from Fairhead et al. (1972), Butzer et al. (1972), Goetz and Hillaire-Marcel (1992) and Röhricht (1998).

alkaline pan, currently floored by trona (Fig. 1). Discontinuous Quaternary sedimentary outcrops around the lake include fluvial sediments (channel deposits, alluvium), calcrete, lacustrine limestone (including microbialites), zeolitic mudstone and siltstone, sodium silicate minerals, and chert of diverse origins (Baker, 1958, 1963; Eugster, 1967, 1969, 1980; Hay, 1968; Herrick, 1972; Surdam and Eugster, 1976; Behr, 2002; Brenna, 2016; Felske, 2016; Leet et al., 2016). These sediments accumulated in a N-S axial rift sump, in which the northern depocentre remained a lake or wetland for most of the last million years because of spring recharge during drier periods. Lake Magadi probably united with Lake Natron in northern Tanzania as a single, relatively dilute lake for different periods during the Pleistocene and early Holocene (Eugster, 1986; Casanova and Hillaire-Marcel, 1987; Williamson et al., 1993).

Lake Magadi was cored in June 2014 by the *Hominin Sites and Paleolakes Drilling Project* (*HSPDP*), which aims to develop basin-to-regional scale palaeoenvironmental histories that can be compared with local hominin remains and artefacts to infer possible environmental influences on hominin evolution (Cohen et al., 2016). We present here results of detailed analyses of the sedimentology, major- and trace-element geochemistry and mineralogy from two Lake Magadi cores and nearby sediment outcrops (Fig. 1A), supported by diatom records, which collectively provide a history of changing aquatic environments during the past million years. Both drill cores reached the volcanic

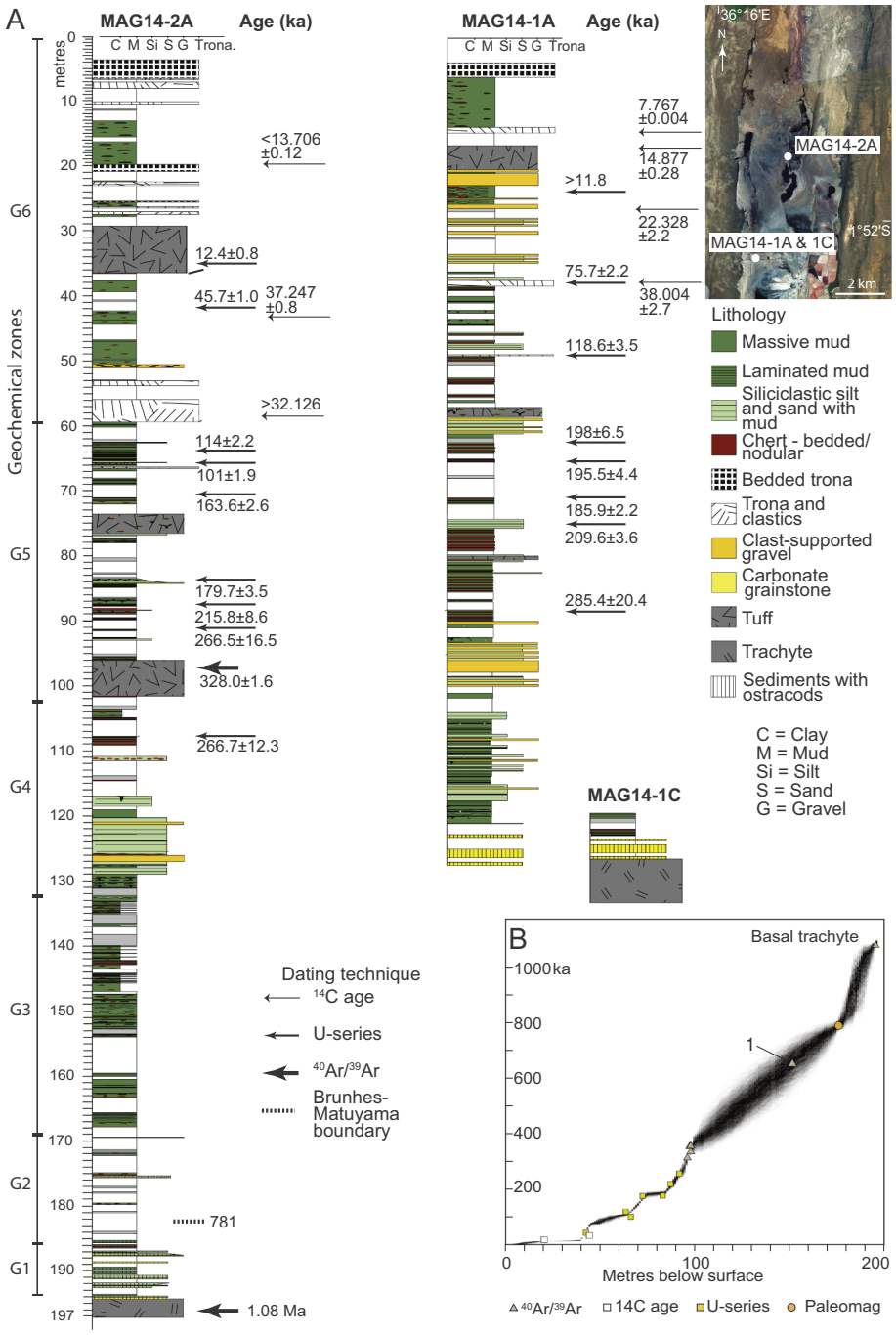

Fig. 2. Core logs of MAG14-2A (drill site 2), MAG14-1A and MAG14-1C (drill site 1) with radiometric ages. A: Major lithologies, ages and dating methods used. B: Bacon Bayesian chronological model from Owen et al. (2018a) who noted that date '1' is 660 ± 37 ka based on a single $^{40}Ar/^{39}Ar$ age that was excluded from the model, but which falls within the predicted trend.

basement. This new evidence gives an opportunity to reconstruct the Pleistocene history of the Magadi basin in much greater detail than previously possible. Specifically, we aim to: 1) reconstruct the environmental history of the Magadi palaeolakes; and 2) relate that sedimentary record to evolving tectonic, volcanic and climatic controls.

2. Previous outcrop and borehole studies in the Magadi Basin

Early descriptions of sediments in the Magadi basin were provided by Parkinson (1914), Gregory (1921), Walter (1922) and Coates (as Anonymous, 1923). The oldest exposed deposits are the fluvial, spring and lacustrine 'Oloronga Beds', which rest upon the Magadi Trachytes (~1.4–0.8 Ma; Fig. 1B; Baker, 1958, 1963; Crossley, 1979, Herrick, 1972; Eugster, 1980; Behr, 2002). A radiometric age of 0.78 ± 0.04 Ma for an obsidian flow overlying basal Oloronga sediments (Fairhead et al., 1972; Eugster, 1980, his Fig. 15.21) is consistent with ^{36}Cl/Cl brine estimates of ~0.76 Ma for salt accumulation in the basin (Kaufman et al., 1990). A U/Th date of 0.3 Ma indicates a minimum age for the 'upper' Oloronga Beds (Fig. 1B; Röhricht, 1998; Behr and Röhricht, 2000), which are overlain by a calcrete (Eugster,

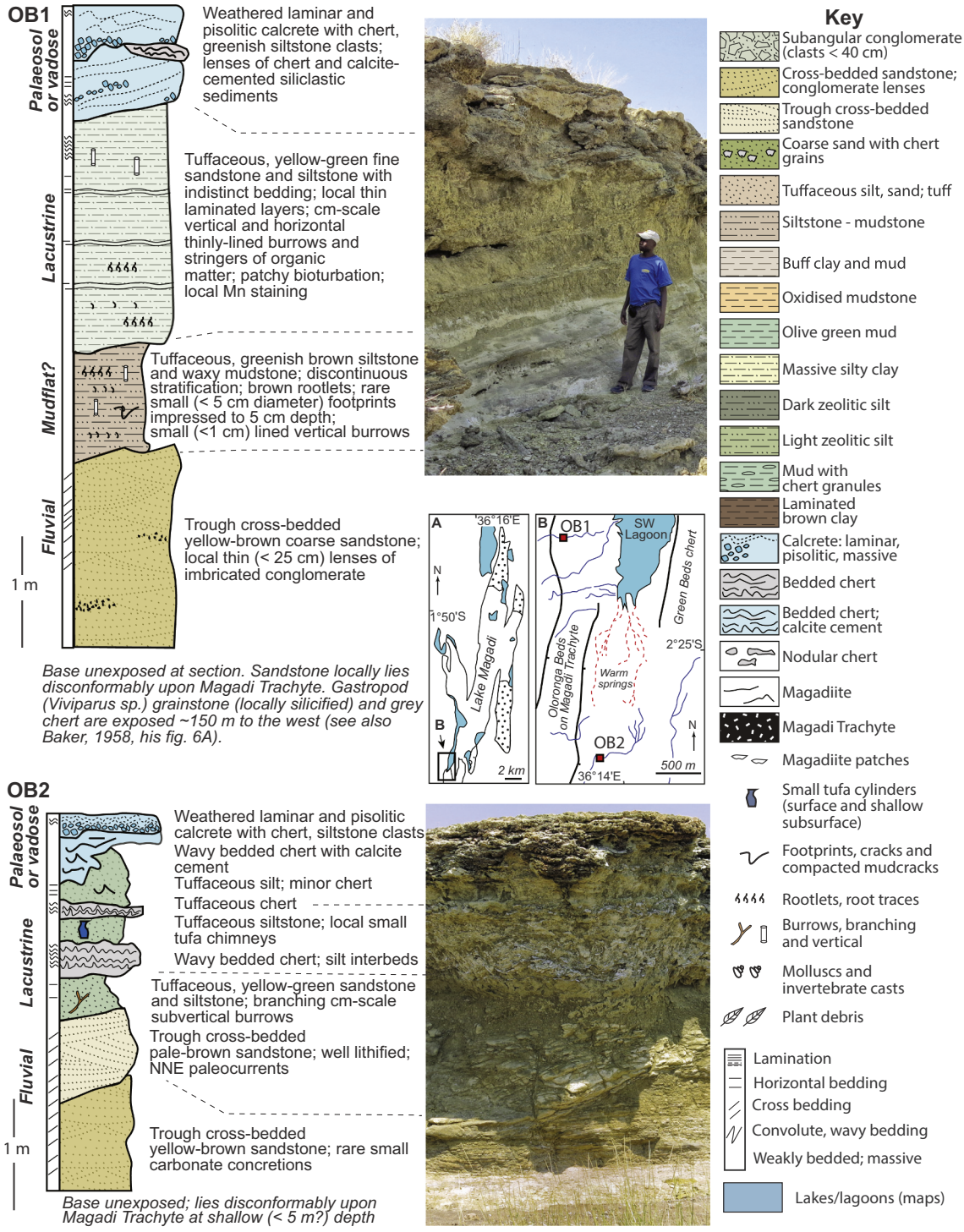

Fig. 3. Oloronga Beds, sections OB1 and OB2 with locations also shown on Fig. 1. Inset maps, A and B, show locations of stratigraphic logs at the southwestern corner of Magadi Basin. Key to all logs in Figs. 3, 5 and 6, to the right. The temporal trend is from fluvial (oldest) to lacustrine and then calcretes.

1980, 1986; Felske, 2016). Lacustrine and alluvial sediments are also preserved several km northwest of Lake Magadi, including at Lainyamok (Fig. 1A) (Shipman et al., 1983; Potts et al., 1988).

Despite a lack of exposure of geological contacts, Temperley (unpublished, cited by Baker, 1958) reported a 'Chert Series' that lay above the Oloronga Beds. Baker (1958) described stratigraphic sections. Eugster (1967, 1969, 1980) and Surdam and Eugster (1976) proposed that the Chert Series formed part of the Late Pleistocene to Holocene 'High Magadi Beds' (HMB), despite their non-conformable contact. U/Th dating of chert by Goetz and Hillaire-Marcel (1992), however, showed that some of the chert deposits were much older (98.5 ± 20 ka and 40.0 ± 6.5 ka). Röhricht (1998), Behr and Röhricht (2000) and Behr (2002) reassigned sediments with bedded chert above the Oloronga Beds to the newly defined 'Green Beds' (Fig. 1B).

Stromatolitic limestones encrusting bedrock up to 60 m above modern Lake Magadi (~660 masl), were used to infer former higher lake-phases at ~130 ka and ~12–10 ka, with a maximum palaeoshoreline at ~656 m (Hillaire-Marcel et al., 1986; Casanova, 1987; Hillaire-Marcel and Casanova, 1987). An earlier stromatolite generation, up to 80 m above Lake Natron, was dated at > 200 ka. Those higher palaeolakes were inferred to have formed a single water body in the combined Natron-Magadi basins.

The Late Pleistocene to Holocene HMB (Fig. 1B) were deposited in the modern axial graben in a fresh to moderately saline, alkaline lake (White, 1953; Baker, 1958, 1963; Eugster, 1969, 1980, 1986; Herrick, 1972; Surdam and Eugster, 1976). White (1953), Baker (1958), Butzer et al. (1972), and Behr (2002) noted a palaeoshoreline ~40 ft (12.2 m) above the modern lake. Partly laminated diatomaceous core sediments dated at 17.71 ± 0.22 to 10.8 ± 0.12 ka from the Northwest Lagoon of Lake Magadi imply freshwater inflow to a former saline lake (Barker et al., 1990; Taieb et al., 1991; Damnati et al., 1992, 2007; Roberts et al., 1993; Damnati and Taieb, 1995).

Baker (1958), Hay (1968), Surdam and Eugster (1976) and Eugster (1980) described the mineralogy of Lake Magadi boreholes drilled in 1953, but gave few stratigraphic details. They inferred low lake-levels after deposition of the HMB, with accumulation of > 40 m of bedded trona and black mud of the Evaporite Series (Fig. 1B). The hydrology, hydrochemistry and brine evolution at Lake Magadi have been discussed by Gregory (1921), Baker (1958), Jones et al. (1967, 1977), Eugster (1969, 1970, 1980, 1986), Eugster and Hardie (1978), Eugster and Jones (1968, 1979), Hillaire-Marcel and Casanova (1987), Allen et al. (1989), Darling (2001) and others. Owen et al. (2018a) described the stratigraphy of the Magadi *HSPDP* cores, upon which this study is partly based, from a palaeoclimate perspective, using pollen, diatom and mineralogical records.

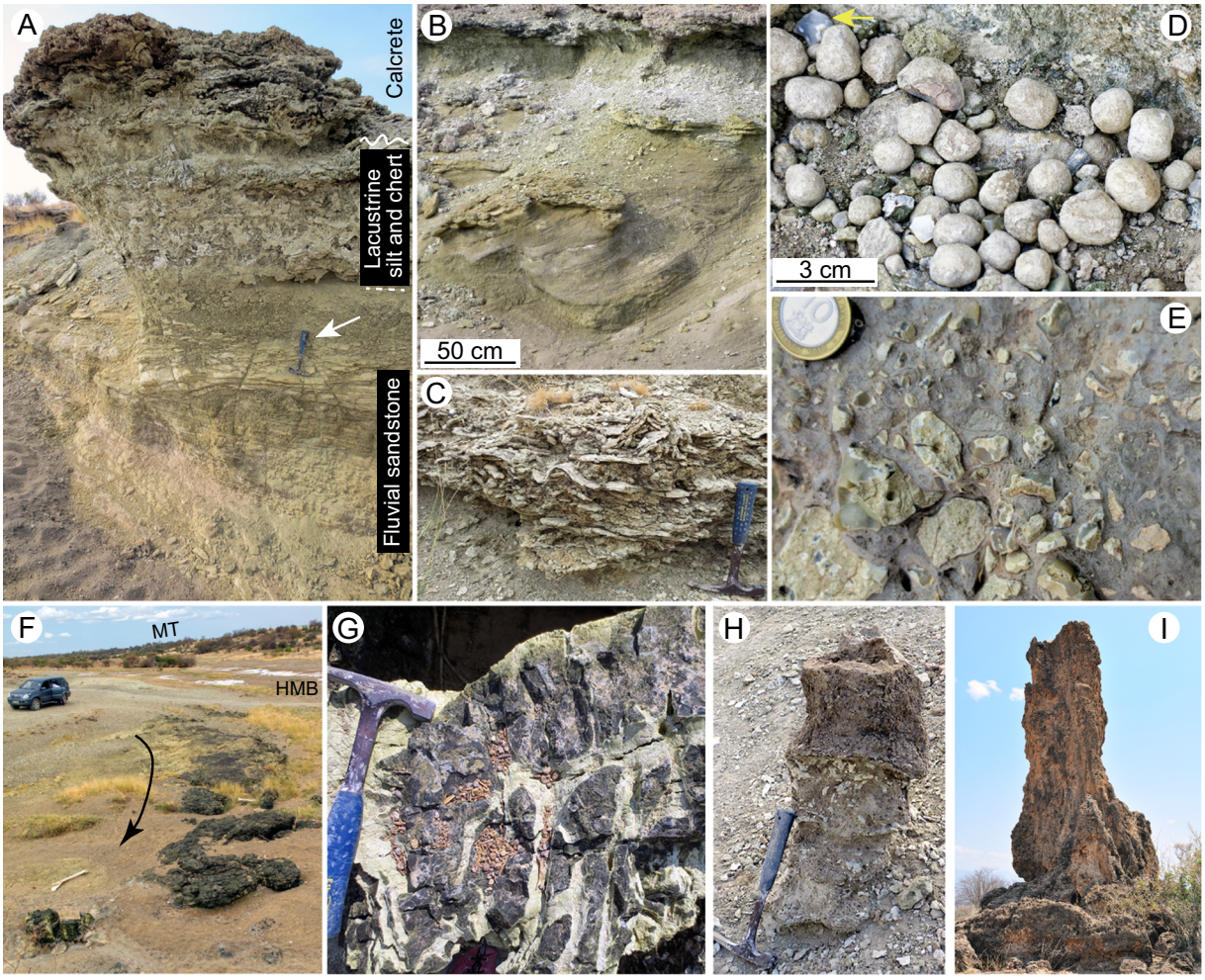

Fig. 4. Oloronga Beds facies in outcrop. Hammer for scale is 28 cm long. A: Basal fluvial sandstone overlain by lacustrine siltstone and chert, with pisolitic and massive calcrete at top, SW Magadi Basin site OB2. B: Detail of trough cross-bedded sandstone in Fig. 4A. C: Thin undulating chert beds in zeolitic siltstone near outcrop in Fig. 4A. D: Uncemented calcite pisoids from depression in capping calcrete, Site OB1. E: Calcrete with chert clasts capping sequence in Fig. 4A; some clasts show reticulation characteristic of Magadi-type chert. Coin diameter: 23 mm. F: Small abandoned palaeochannel filled with greenish black claystone near Site OB2. HMB: tuffaceous siltstone of upper High Magadi Beds; MT: Magadi Trachyte escarpment. G: Fossil branching root-system in greenish black claystone (F) filled by younger fine silts. H: Small cylindrical tufa chimney in zeolitic siltstone and chert near section OB2. Calcite lip around top implies that the small spring vent was subaerially exposed at times. I: Tufa tower, ~6 m high, located < 80 m from the western edge of a NNE-SSW horst, ~7 km west of Lake Magadi.

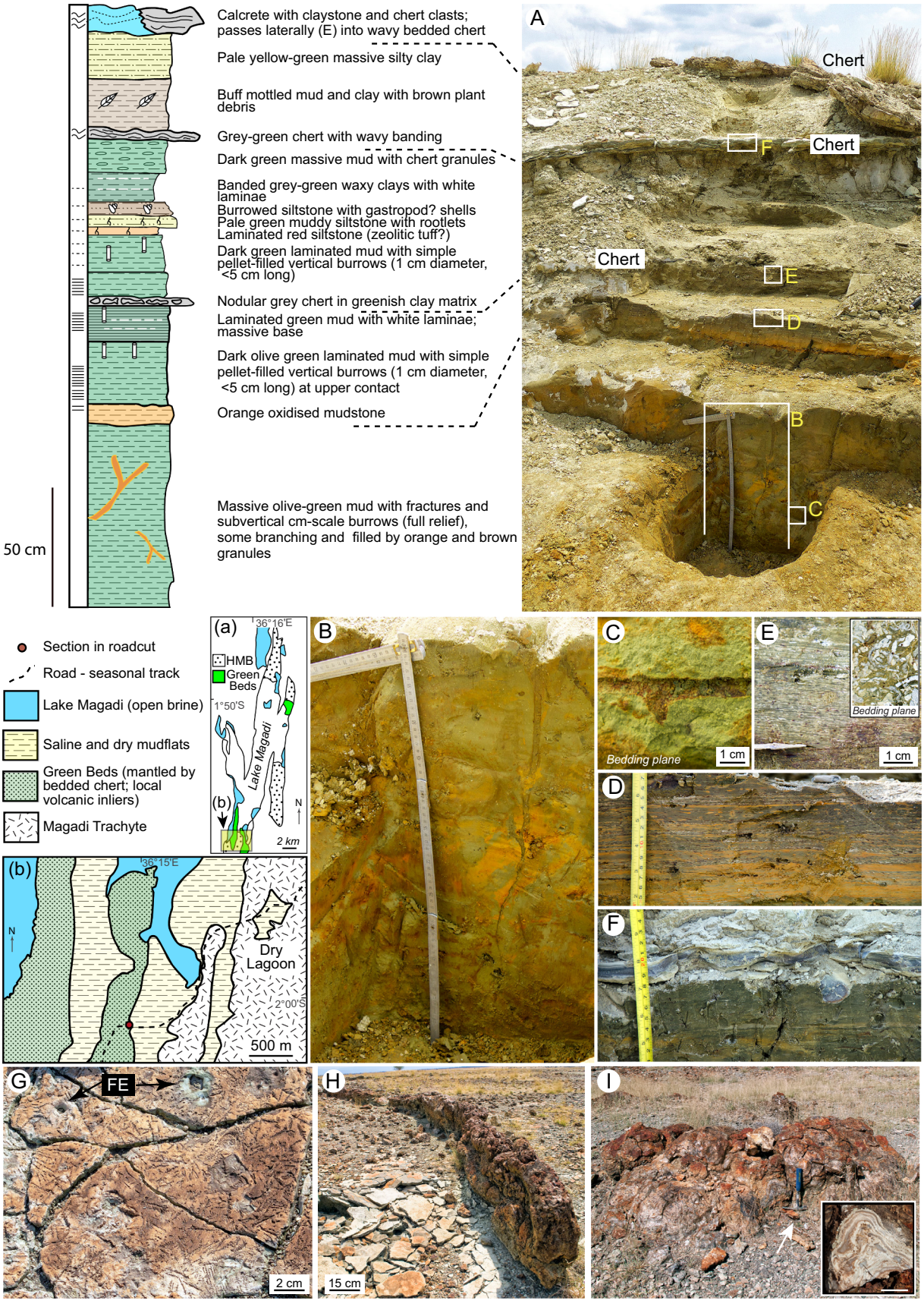

(caption on next page)

Fig. 5. Section GB1 of Green Beds, south Lake Magadi. See Fig. 3 for the key. Inset maps (a, b) show location of the section, excavated on the northeastern edge of the track crossing a prominent N-S ridge (horst) armoured by bedded Green Beds chert. A: Exposed section showing context of facies photographs in images B to F. B: Lowest part of the section showing burrowed and mottled pale green and orange mud with prominent straight thinly lined vertical burrow preserved in full relief and partly filled by orange and brown granules. C: Horizontal burrow with short blunt side-branches on bedding plane in lower part of section. Preserved as negative epirelief. Burrow fill is finer than host sediments. Similar burrows, horizontal and vertical, are common also in Oloronga Beds outcrops. D: Weakly laminated green and orange muds, locally mottled, with lenses of pale grey mud. E: Grey-green and white 'laminated' muds. The discontinuous white laminae, 1–2 mm thick, comprise patches of compacted plant debris and (or) trails mineralised by opal-A? (see inset, same scale). Although they appear to be white laminae in section they are discontinuous. F: Thin chert bed with low-amplitude undulations overlying dark green muds. G: Outcrop of horizontally bedded chert showing crystal pseudomorphs (moulds) of carbonate minerals and fluid-escape structures (FE) that confirm a soft precursor. Eugster (1969) termed these linear moulds "pearl chains of calcite rhombs and their casts", suggesting they were originally calcite or gaylussite. H: Chert dyke, up to 80 cm high, cutting older, platy bedded chert (left). I: 'Pillow chert' of Behr (2002). These common cherts form coalescent, mainly reddish mounds several metres long (typically oriented N-S) with brecciated chert interiors covered by fractured, laminar chert layers (inset: scale bar: 3 cm) producing a biohermal morphology. Arrow points to hammer ~ 30 cm long. (For interpretation of the references to colour in this figure legend, the reader is referred to the web version of this article.)

3. Methods

Sediment outcrops logged between 2006 and 2018 were combined with sampling of modern sediments and waters across the catchment. Lake Magadi was drilled in June 2014 to depths of ~133 mbs (metres below surface; Site 1) and 194 mbs (Site 2) (Fig. 1A; Cohen et al., 2016). Geochemical analyses were carried out on outcrop samples (n = 76) and core sediments, with MAG14-2A sampled at 32 cm intervals, and where distinctive lithologies would have been omitted (n = 344; see Electronic Supplementary Material). Samples were analysed by Activation Laboratories Ltd., Ancaster ON, Canada (4E-exploration package; for methods, see http://www.actlabs.com). Major and trace elements were determined by coupled-plasma and inductively coupled plasma-mass spectrometry. Detection limits are given in the Electronic Supplementary Material. Rare earth element (REE) data were normalised against C1 chondrite composition (Sun and McDonough, 1989). Total organic-carbon (TOC) was determined by loss-on-ignition (LOI) at 550 °C without prior removal of carbonates. X-ray diffraction samples were taken at 16 cm-intervals and analysed using a Panalytical X'pert Pro MPD diffractometer using CuKα radiation at 45 kV and 40 mA.

Diatoms are rare or absent in outcrops. In MAG14-2A, diatom samples were collected every ~32 cm (as for geochemical samples) and where facies changed. Synthetic silica microspheres (8 μm diameter) were added to assist quantitative counts. Organic matter and carbonates were removed using H_2O_2 and HCl. Diatoms were mounted in *Naphrax*. At least 400 frustules were counted for each microscope slide except where diatoms were rare (see Electronic Supplementary Material).

Dating methods are described by Owen et al. (2018a). Chert samples from core (n = 18) and outcrop (n = 6) samples were dated using U-series methods (Fig. 2A). The uppermost parts of the cores were dated using ^{14}C techniques (n = 11). Those analyses produced inconsistent ages, likely because of recycled old carbon; six ages are compatible with the lithostratigraphy. Nine replicate $^{40}Ar/^{39}Ar$ single-crystal dates were determined from K-feldspar crystals in a little-altered tephra in MAG14-2A at 96–101 mbs with a single crystal date obtained at 151 mbs. The Brunhes-Matuyama boundary was identified at 174.36 mbs. Bayesian methods were applied to define the age-model and its uncertainties (Fig. 2B; Bacon v. 2.2; Blaauw and Christen, 2011).

4. Results

4.1. Exposed Quaternary sediments

The Early to Middle Pleistocene Oloronga Beds overlie Magadi Trachyte in scattered outcrops north, south and west of Lake Magadi (Baker, 1958; Fig. 1A). Sections OB1 and OB2, southwest of Magadi, contain trough cross-bedded fluvial sandstone (Figs. 1A, 3, 4A, B) overlain by bedded, wavy lacustrine chert and grey zeolitic siltstone (Fig. 4C) covered locally by thin (< 5 cm) dark grey limestone. A laterally extensive calcrete up to 40 cm thick, with massive, pisolitic and laminated facies caps the Oloronga Beds disconformably across much of the basin (Fig. 4A, D; Eugster, 1980; Felske, 2016), including at Section OB2 where the massive facies contains subangular chert clasts (Fig. 4E). This calcrete is one of several of different ages (Felske, 2016). Locally, SW-NE palaeochannels that incise the fluvial sandstone are filled with blackish brown mudstone with lighter cm-scale subvertical and horizontal branching trace fossils (roots?) (Fig. 4F, G).

Small cylindrical pale grey-brown tufa 'chimneys' (< 70 cm high, < 40 cm diameter, ~1 cm-thick walls) with a flat upper rim are interstratified with grey silts and laminar cherts at sites < 150 m from the modern SW Magadi hot springs (Fig. 4H). The calcite tufa cements angular chert and siltstone fragments. Most chimneys align along N-S to NNE-SSW trends.

About 10 km west of northern Lake Magadi (Fig. 1A), several tall N-S–aligned tufa towers up to ~6 m high (Fig. 4I), and linear mounds of spring carbonate (up to ~2.5 m high with variable orientation), lie upon Magadi Trachyte (Baker, 1958). Internally, most towers are composed of clusters of cm-scale vertical pipes with subhorizontal plates and cement. About 150 m south of the tallest mound (Fig. 4I), poorly-preserved rimstone dams are present. These spring deposits lie ~120 m east of a fault-scarp up to 20 m high that marks the edge of the N-S horst upon which the towers are rooted.

Section GB1 (Fig. 5), located at the southern margin of Lake Magadi (Fig. 1A), exposes a 2.6 m sequence of Middle to Late Pleistocene Green Beds (Fig. 5A). The section includes basal massive, burrowed green and orange mud (Fig. 5B, C) that gives way upwards to laminated green and orange mud with thin white flakes (silicified plant fragments?) on lamination planes (Fig. 5D, E), thinly shelled spired gastropods, and three bedded, undulating light and dark grey quartz-chert horizons < 3 cm thick (Fig. 5F). The latter can be traced northwards for > 700 m and E-W for > 100 m and, on the land surface, show open crystal moulds of calcite, trona, gaylussite and other salts (Fig. 5G), fluid-escape structures, shrinkage cracks, tepee structures, trace fossils and possible raindrop-impact prints (Eugster, 1969; Behr, 2002; Scott, 2010). Northeast of the lake, low (< 30 cm) terraces of pale-green chert fragments might reflect palaeoshorelines of unknown age. Many chert precursors (opaline species, gels or sodium silicates?) were remobilised while partly soft to form dykes, decimetres thick and at least 50 m long (Fig. 5H). Other intrusive chert outcrops consist of reddish domal mounds of quartz with concordant fractured and brecciated laminae, some with couplets and triplets of repeating laminae typical of microbialites (Fig. 5I).

Palaeoshorelines that formed when Lake Magadi was a deeper expanded lake are present in many locations up to ~12 m above the modern lake (Figs. 6, 7A–B). Exposures in the 'Dry Lagoon' southeast of Lake Magadi (Fig. 1A) show sections through the Late Pleistocene to Early Holocene HMB (Fig. 6). The Lower HMB include a basal imbricated trachyte breccia (subangular conglomerate) overlain by interbedded gravel lenses and pale brown tuff with thin lensoid to bedded magadiite horizons and isolated magadiite patches. The top of the lower HMB in many outcrops is a dark brown, laminated clay with well-preserved *Tilapia* fish fossils (Fig. 7D). In contrast, the Upper HMB are a crudely to well-bedded, zeolitic (mainly erionite) tuffaceous silt.

Volcaniclastic trough-cross-bedded sandstone overlain by Upper HMB near Karamai (SE Magadi) provides evidence of fluvial-deltaic inflow to the palaeolake (Figs. 6D, 7C).

Trona, which covers Lake Magadi during most dry seasons (Fig. 7E, F), is the contemporary surface of the Evaporite Series (Baker, 1958), which comprises bedded and massive trona and nahcolite, interbedded with anoxic black zeolitic mud. The evaporites and mud extend > 65 m below the lake floor.

4.2. Core data

4.2.1. Sedimentology and mineralogy

Cores MAG14-1A and MAG14-1C form a composite sequence that reached trachyte at 133 mbs. MAG14-2A contains 194 m of sediment, including gaps (Figs. 1A, 2A). Core sediments consist of detrital siliciclastic grains, primary (airfall) and reworked ash and pumice, detrital and authigenic clay minerals and zeolites, carbonate (micrite, gastropods, ostracods), siliceous microfossils (diatoms, sponge spicules, phytoliths) and organic matter (pollen, spores, charcoal, diffuse organic matter, microbial matter). Evaporite deposits, common in the uppermost 65 m of MAG14-2A, include nahcolite and abundant trona. Calcite, Mg-calcite and dolomite are present below ~100 mbs. Many minerals, both deposited and precipitated, have undergone early diagenetic alteration. Zeolites, including erionite, phillipsite, mordenite, natrolite, clinoptilolite, chabazite and analcime, are common, especially between ~100 and 10 mbs. K-feldspar, clay minerals, biotite, pyrite and hematite are also common. Chert (as cryptocrystalline quartz and chalcedony) and magadiite are present at some levels.

Fifteen lithofacies are distinguished (Table 1; Fig. 8). Gastropod- and ostracod-bearing carbonate-grainstone are present in the basal parts of both cores (Facies 1–3, Table 1). Overlying sediments are zeolitic, massive, thinly bedded or laminated, green, brown or black silt, clay, mud and ash (F4–F8, Table 1, Fig. 8). Nodular and bedded chert (F13) and silicified mudstone (F12) are also present. Massive (F11) and bedded (F10) trona, and massive black, zeolitic mud with trona (F9) dominate the uppermost 65 m of core MAG14-2A.

Coarse-grained siliciclastic sediments include matrix-supported paraconglomerate and rare sand-and-gravel (orthoconglomerate) intervals (F15), which are most common in MAG14-1A. Palaeosols are absent, but minor root development was observed (F14).

4.2.2. Geochemical zonation, MAG14-2A

Correlations between outcrops and geochemical zones are shown in Fig. 9. Six geochemical zones (G1–G6) can be distinguished using changes in total organic carbon (TOC) and Ca/Na and (K + Na)/Al ratios (Fig. 9A). TOC is low and Ca/Na ratios are highest in Zone G1 (194.3–186 mbs, ~1056–930 ka; Figs. 2, 9A). Ca/Na ratios and (K + Na)/Al decrease in G2 (186–169 mbs, ~930–740 ka), but P_2O_5 concentrations increase. Calcite is present throughout both zones with analcime confined to G1, and Mg-calcite present in lower G1. Zone G3 (169–132 mbs, ~740–545 ka) includes variable Ca/Na and slightly elevated (K + Na)/Al ratios. Calcite is present throughout, with Mg-calcite common, and dolomite recorded at some levels. Analcime is present through most of G3 but other zeolites are absent. Zone G4 (132–102 mbs, ~545–380 ka) has variable Ca/Na ratios but with a moderate increase in (K + Na)/Al. Calcite and Mg-calcite are present, but less common than in Zone G3. Zeolites other than analcime appear for the first time in a few horizons in G4. Zone G5 (102–60 mbs,

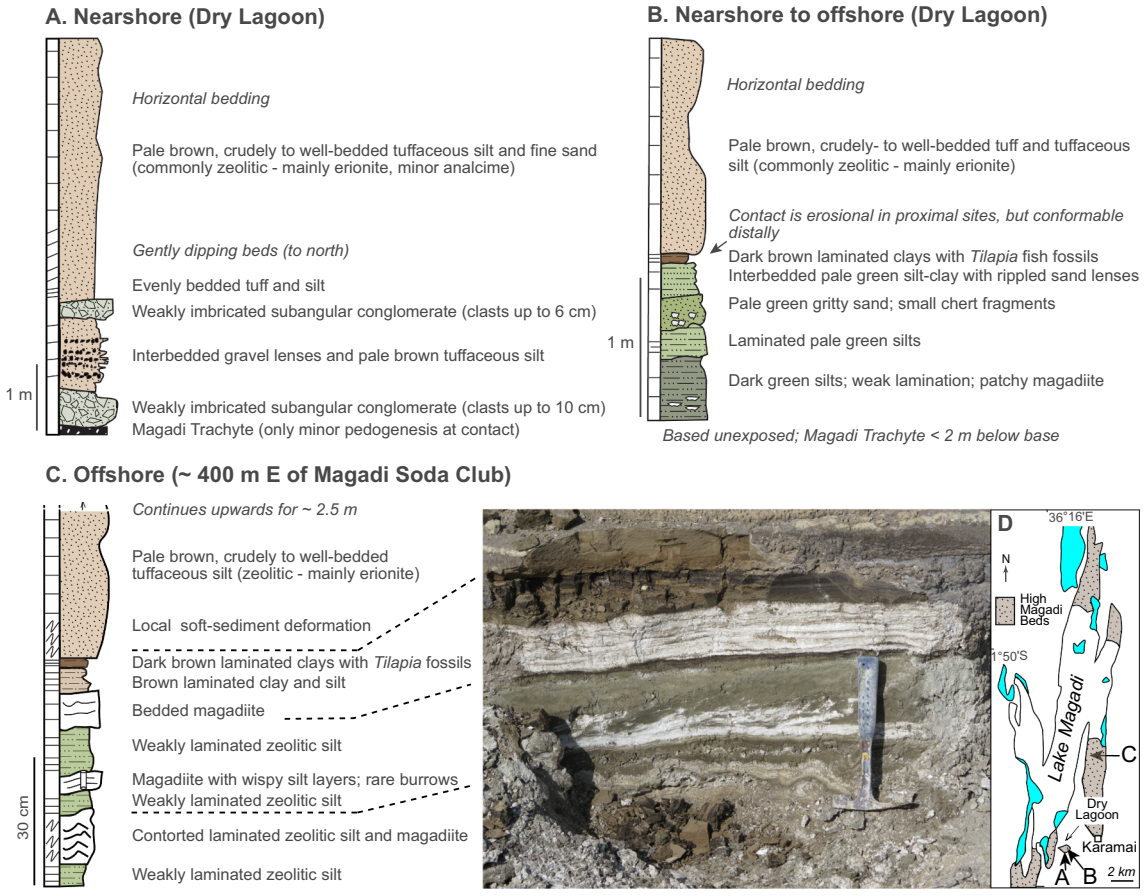

Fig. 6. Sections of the High Magadi Beds showing relative nearshore (A), nearshore to offshore (B) and offshore (C) outcrops in the southeastern margin of the contemporary palaeolake Magadi. Note trend from coarse-grained sediments to bedded and laminated sediments with magadiite in offshore locations. No known outcrops preserve the finer deeper-water facies recorded in axial cores. See Fig. 3 for the key.

Fig. 7. Late Pleistocene and Holocene sediments. A: Late Pleistocene to Holocene High Magadi Beds' palaeoshoreline (arrow), about 12 m above modern Lake Magadi. Location is ~1.3 km east of Magadi townsite with people for scale. B: Thin hemispheroidal stromatolitic crust (calcite) on trachyte pebble along the +12 m palaeoshoreline, midwestern shore of Nasikie Engida. C: Trough cross-bedded fluvial sandstone at the southern end of the graben east of Magadi townsite (Karamai). View towards northwest. This sandstone may record fluvial and deltaic channels flowing into the HMB palaeolake. D: High Magadi Beds sediments including bedded gravel, silt and magadiite overlain by well-bedded, *Tilapia*-bearing clay, with slumped silt at top. A 4-m-thick, bedded zeolitised ash caps the sequence. Central Dry Lagoon at southeastern Magadi. E: Exposed surface of the Holocene Evaporite Series formed mainly by trona, with *HSPDP* drilling platform (Core MAG14-1A). F. Bedded trona forms the modern surface crust. Two units of bottom-nucleated upward-expanding trona-fans are separated by a muddy layer recording a flooding surface with fine clastic deposits and brown organic matter. Syntaxial crystal growth continued through that detrital surface into the overlying crystal bed.

~380–105 ka) is characterised by low Ca/Na and (K + Na)/Al ratios and LOI values that intermittently increase in upper G5. Calcite and Mg-calcite are absent, but a more varied assemblage of zeolites is present. Zone G6 (60–0 mbs, ~105–0 ka) shows an increase in TOC, low Ca/Na ratios, and very high (K + Na)/Al ratios, reflecting the dominance of trona and nahcolite. The dominant zeolites vary in G6. Using trace elements, nineteen subzones are recognised (Fig. 9B; Table 2).

4.2.3. Diatom stages

Fig. 10 shows selected diatom taxa in core MAG14-2A plotted against age, highlighting periods when diatoms were preserved between ~545 and ~16 ka (132–38 mbs). Correlations with outcrops are also shown in this figure. Nine stages are distinguished. Stages D1 (194.3–132 mbs, ~1056–545 ka) and D9 (37–0 mbs; ~16–0 ka) lack diatoms. Both saline (e.g., *Thalassiosira faurii*, *T. rudolfi*, *Cyclotella meneghiniana*) and freshwater (*Aulacoseira granulata* and varieties, *A. agassizii*) taxa are present in D2–D8 sediments. Stage D2 (132–108 mbs, ~545–415 ka) contains rare diatoms dominated by planktonic *Aulacoseira* spp., but with *C. meneghiniana* and *T. faurii* recorded in a few horizons. Overall diatom diversity is low. Diatoms vary in abundance in D3–D8 and include well-preserved diverse floras with episodic increases in benthic taxa. Stages D3 and D5 are distinguished by abundant *C. meneghiniana*. Planktonic *A. granulata* and *A. agassizii* are common throughout D3–D8, with the former dominant in most samples from D4, D6 and D8 and the latter dominant in D3 and D7.

5. Discussion

5.1. Palaeoenvironmental interpretation

5.1.1. Geochemical stratigraphy

Lacustrine deposition began soon after volcanic eruptions in the Magadi Basin ceased, given the lack of weathering of the underlying trachytes. Zone G1 (~1056–930 ka) is characterised by ostracod-rich grainstone without diatoms. In contrast, ostracod- and gastropod-rich grainstone in the basal part of MAG14-1A and MAG14-1C (Fig. 2A) contains freshwater benthic and epiphytic diatoms (*Epithemia*, *Rhopalodia*, *Encyonema*), implying a marsh setting. Grainstone is absent above the G1-G2 boundary, but calcite in silts throughout G2 (~930–740 ka) indicates relatively low palaeolake salinity. Calcite might have formed during photosynthetic microbial blooms as happens in modern rift lakes (cf. Ng'ang'a et al., 1998; Stone et al., 2011).

Principal component analyses confirm a close relationship among REE, Al_2O_3, Fe_2O_3 and TiO_2 and feldspars, implying similar detrital sources (Fig. 11A). REE patterns for G1 and G2 resemble those for the Magadi Trachyte Formation (Fig. 11B), which are characterised by a

Table 1
Representative major facies. See Fig. 8 for typical examples in core. Based on *HSPDP* Initial Core Description (ICD) logs. Letters refer to facies codes.

Primary lithology	Facies code	Lithology, structure and diatom content	Associated features	Environmental interpretation
F1. Gastropod limestone	Lg	Limestone (L) with abundant in situ and reworked gastropod (g) shells in micritic and sparitic matrix.	Shallow-water diatoms, ostracods.	Shallow to moderately deep, fresh lakes.
F2. Carbonate grainstone	Lgr	Bedded fine to coarse carbonate sand grainstone (shells, trachyte) (r). Weakly laminated in a few horizons.	Shallow water diatoms, ostracods, gastropods.	Shallow to moderately deep, fresh lakes.
F3. Carbonate mud	Lu	Poorly bedded, light brown carbonate mud (u).	Black pyrite grains (1–1.5 cm) with bluish rims. Light coloured grains of chert. Chert with open vugs.	Moderately deep or deep, fresh to mildly saline lake.
F4. Laminated silt and clay	Czl	Greenish grey, light brown or brown zeolitic or calcitic silty (z) clays (c). Laminae (l) 1–3 mm thick.	Convolute laminae, microfractures. Pollen. Pyrite, patchy chert, unidentified white crystals.	Lacustrine.
F5. Bedded silty clay	Czb	Alternating beds (1–6 cm thick) (b) of light to medium and darker green zeolitic silty clay (C) or clayey silt. Darker bands are siltier.	Scattered pyrite. Mottling. Unidentified white crystals.	Lacustrine.
F6. Massive clay	Cm	Massive (m) to weakly bedded light green zeolitic clay. Wispy banding (1–4 cm).	Scattered white crystals and pyrite. Also present in subhorizontal wisps and laminae (1–2 mm).	Lacustrine.
F7. Massive silty ash	Zm	Massive (m) dark grey zeolitic silt (Z). Subhorizontal fractures hint at layering.	Local chert nodules. Pyrite in some levels.	Lacustrine.
F8. Black clay	C	Massive to weakly laminated clay (C). Locally alternating with each other at cm scale. Diffuse organic matter; rare plant fragments. Fine clastic grains.	Scattered and lensoid wisps of white (calcite?) crystals, locally in laminae. Scattered pyrite, also in laminae. Chert nodules.	Lacustrine.
F9. Massive mud with trona	Mt	Black mud (M) with mm-scale trona (t) crystals. Interbedded with massive or bedded trona.	Some larger trona crystals.	Saline alkaline lake.
F10. Bedded trona	Tb	Bedded trona (T) (1–3 cm layers) with clusters of radiating crystals.	(Sub)horizontal dissolution surfaces.	Very shallow (< 1 m?), saline, alkaline lake.
F11. Massive trona	Tm	Massive recrystallized trona. Crystals < 1 to 3 cm with mostly random orientations.	Interstitial greenish black mud is common.	Saline alkaline lake.
F12. Silicified mudstone	Ui	Bedded green mud (U) with variable degrees of silicification (i). Very fine clay with some silt.	Pyrite present at some levels.	Lacustrine.
F13. Chert	Hb; He; Hn	Bedded (b), lensoid (e) to nodular (n) cherts (H).	Compaction around chert indicating early lithification. Some chert has serrated or reticulate surface textures.	Shallow saline lake. Replacement of magadiite, trona, mudstone or silica gel in saline lake sediments.
F14. Massive mud with roots	Umr	Massive green mud with plant remains, roots (r) and local oxidation.	Pyrite.	Palaeosol, but with reducing conditions dominant?
F15. Sand and gravel (bedded or massive)	Gsb/m	Bedded sand (s) and gravels (G). Rarely graded.	Locally forms paraconglomerates.	Alluvial sandflat with local debris flows?

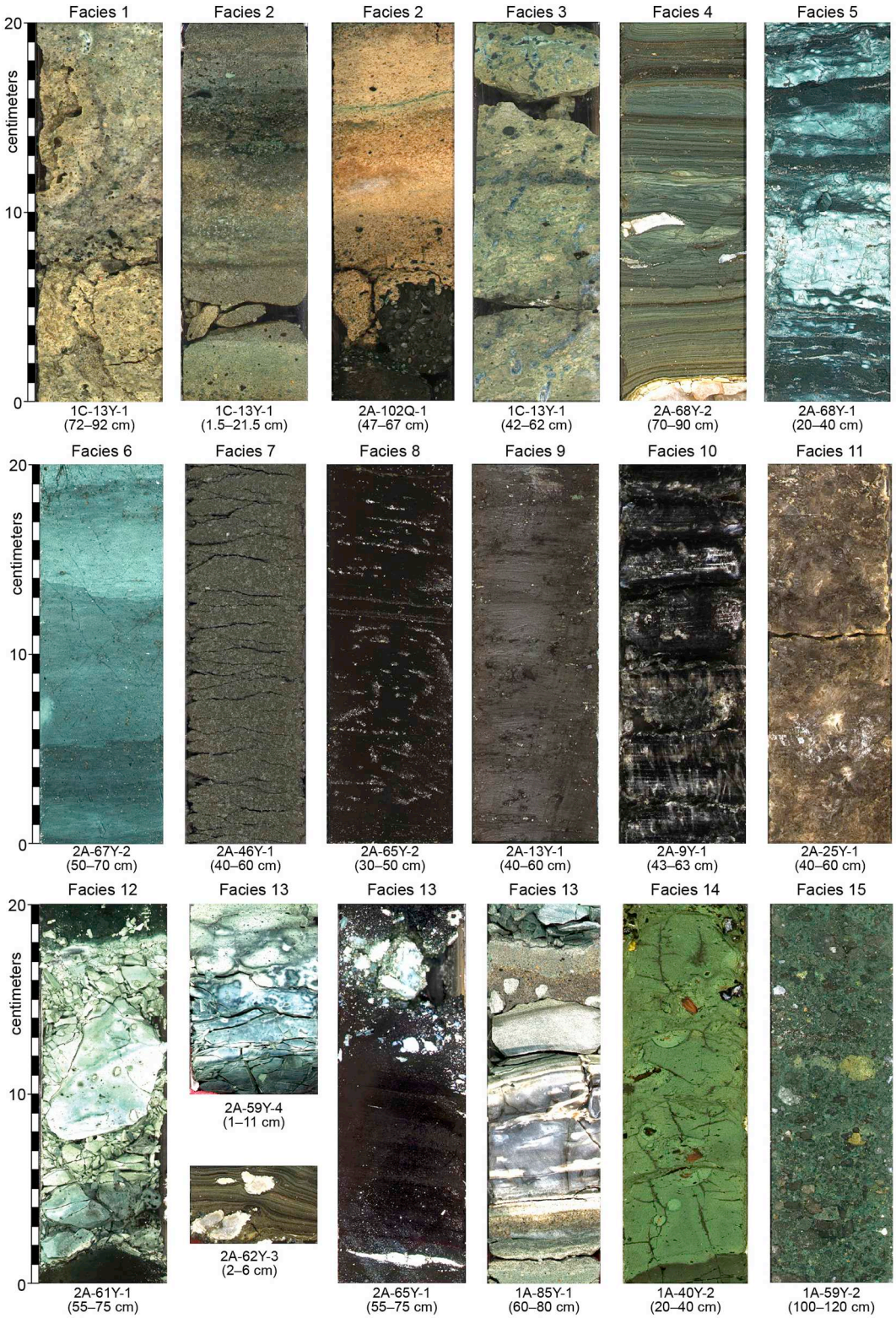

Fig. 8. Major lithofacies preserved in cores: see Table 1 for descriptions. Core segment and segment depth for each section is shown below each photograph. F1: Gastropod limestone. F2: Carbonate grainstone. F3: Carbonate mud. F4: Laminated silt and clay. F5: Bedded silty clay. F6: Massive clay. F7: Massive silty ash. F8: Black clay. F9: Massive mud with trona. F10: Bedded trona. F11: Massive trona. F12: Silicified mudstone. F13: Bedded chert (59Y-4; 85Y-1). Nodules in laminated silts (62Y-3) and in black mud (65Y-1). F14: Massive mud with roots. F15: Sand and gravel.

negative Eu anomaly that is absent in basalts of the region (Le Roex et al., 2001; Owen et al., 2011, 2014). Furthermore, low concentrations of Co, Cr, Cu, Ni and V (Fig. 9B) support a trachytic source lithology because these transition metals are less abundant in lavas of the Magadi Trachyte Formation (2.6–3.9, 1.6–4.9, 6.3–12, < 8.4, < 3 ppm, respectively) than in rift basalt (41–51, 53–254, 110–184, 21–124 and 232–307 ppm, respectively) (Le Roex et al., 2001).

Zones G1 and G2 are also distinguished by relatively high P_2O_5.

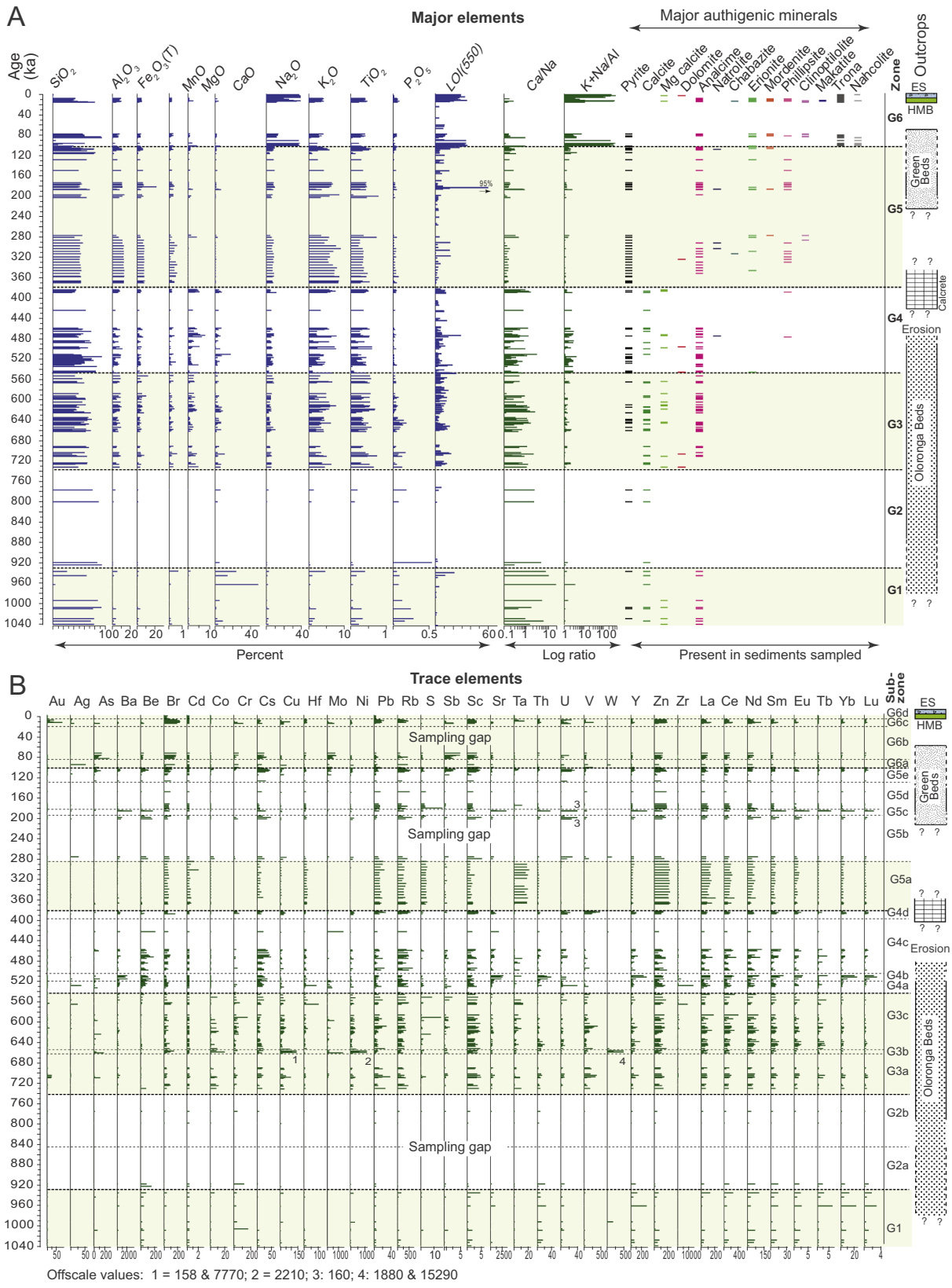

Fig. 9. Geochemical zones (bulk geochemistry) and authigenic mineralogy versus time for core MAG14-2A. A: Geochemical zones are based on changes in Ca/Na and (K + Na)/Al ratios, P_2O_5, LOI and mineralogy and broadly reflect a transition from fresh and mildly saline waters (G1 to G3) to saline (G4) and hypersaline (G5 and G6) conditions. Major authigenic minerals to right (excluding silica species: quartz, chalcedony, magadiite and other sodium silicates, which are present at several levels). Siliciclastic detrital minerals are shown in Table 2. B: Temporal variability in trace elements, Core MAG14-2A. Subzones are defined using trace elements (Table 2) and reflect changes in salinity of the palaeolake, spring inputs, variations in bottom water conditions and the supply of transition metals from basaltic and trachytic lithologies. All elements in ppm, except for Au (ppb) and S (%). See Table 2 for descriptions of each zone and subzone. Magadi outcrop correlations shown to the right (ES = Evaporite Series; HMB = High Magadi Beds). Green Beds dating range includes younger dates from Behr (2002) and results from this study (191–158 ka).

Table 2
Geochemical zones in the Lake Magadi cores (HSPDP): distinguishing features and sedimentary characteristics.

Zone	Sub zone	Age (ka)	Major elements	Trace elements	Major lithologies	Mineralogy/LOI
G6	d	5–0	Low Ca/Na ratios; moderate to very high K + Na/Al; high LOI; low P_2O_5, CaO and MgO; relatively low Al_2O_3, SiO_2	Low trace-element concentrations	Trona and black anoxic mud	Mg-calcite and dolomite near top of core; trona, nahcolite, pyrite, quartz, albite, anorthoclase, K-feldspar, analcime, natrolite, mordenite, erionite, phillipsite, chabazite, clinoptilolite, natrolite. High LOI
	c	28–5		Variable moderate to elevated Au, Ag, Br, Cr, Cu, Mo, Pb, Rb, Sb, Ta, V and Zn		
	b	82–20		High As, Br, Mo, Sb. Generally low REE values		
	a	100–82		Most trace-element concentrations lower than subzones below or above. Low REE values. High Sn in one horizon		
G5	e	130–100	Low Ca/Na ratios; moderate K + Na/Al; low to moderate LOI (with one very high value); low P_2O_5, CaO and MgO	Relatively high As, Be, Br, Cs, Mo, Rb, Sb, Sc and U compared to G5d	Siliciclastic silt, sand and mud; chert, tuffs	Pyrite, quartz, albite, anorthoclase, K-feldspar, analcime, erionite, phillipsite, natrolite. Low LOI
	d	181–130		Low Ba, Be, Cs, HREE. Other elements similar to G5c except increased Zn		
	c	192–181		Elevated Ba, Be, Sr, Th, U and HREE		
	b	285–192		High Be, Cs, U, Sc and Ag near base. Other elements similar to G5a except low Ta and moderate Zn		
	a	375–285		Low As, Ba, Cr, Mo, Ni, Sr, U, V and HREE with elevated Ta and Zn		
G4	d	395–375	Similar to G3 but with higher K + Na/Al	Elevated Sc, V compared to G4c	Siliciclastic silt, sand mud and chert	Calcite, Mg-calcite, dolomite, pyrite, quartz, albite, anorthoclase, K-feldspar, feldspathoids, erionite, analcime, phillipsite, natrolite. Low LOI
	c	505–395		Similar to G4b, but with lower Ba, Sr, Th, Y and variable REE		
	b	520–505		Increased Ba, Be, Cs, Sr, Ta, Th and Y; elevated REE		
	a	545–520		Co very low. Slight increase in Ba, Be and U compared to G3c		
G3	c	650–545	Low to moderate Ca/Na ratios; moderate K + Na/Al; low P_2O_5; moderate LOI, CaO and MgO	Similar to G3a, but with Be increasing upwards	Siliciclastic silt, sand and mud and chert	Calcite, Mg-calcite, dolomite, pyrite, quartz, albite, anorthoclase, K-feldspar, feldspathoids. Low LOI
	b	660–650		Elevated Br, Co, Cu, Mo, Ni and W, with lower REE compared with G3a		
	a	730–660		Increased Co, Pb, Rb, Ta, Zn and REE compared to G2b		
G2	b	845–730	Moderate to high Ca/Na ratios; low K_2O + NaO/Al_2O_3 and LOI; low to high P_2O_5; low CaO and MgO	Low trace-element concentrations	Mud, chert	Calcite, pyrite, quartz, albite, anorthoclase, K-feldspar, analcime. Very low LOI
	a	930–845		Low trace-element concentrations. Slightly elevated Th, Y, Zn, Zr and REE		
G1	1040–930 ka		Very high Ca/Na ratios; low K_2O + NaO/Al_2O_3; low to moderate LOI; high P_2O_5; moderate to high CaO but low MgO	Trace elements low; Moderately high Be, Cr, Rb, Sc and REE	Carbonates, siliciclastic mud and chert	Calcite, Mg-calcite, dolomite, pyrite, quartz, albite, anorthoclase, K-feldspar, feldspathoids, analcime. Very low LOI

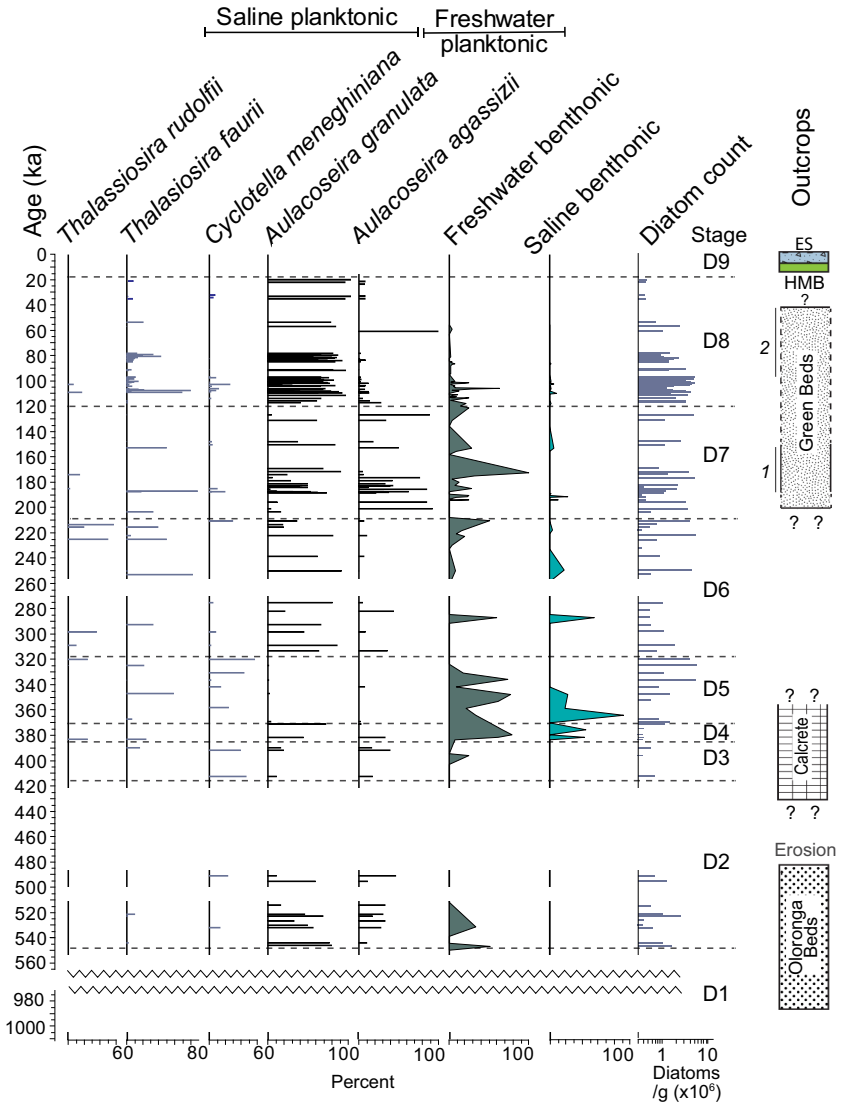

Fig. 10. Diatom stratigraphy of Core MAG14-2A. A total of 62 taxa were recorded from which five dominant planktonic diatoms are plotted together with total freshwater and total saline benthic taxa. Nine diatom stages are recognised based on the presence or absence of diatoms, percentage of saline taxa (*Thalassiosira* spp., *Cyclotella meneghiniana*) and the presence of freshwater *Aulacoseira granulata* versus freshwater *A. agassizii*. Divisions are also based on the occurrence of benthic taxa. The floras show mixing of saline and planktonic species with episodic increases in saline and freshwater benthic taxa. Mixing of planktonic floras reflects the development of saline, fresh and meromictic lakes with benthic freshwater taxa possibly introduced to the core site during floods. Outcrop correlations are shown to the right (ES = Evaporite Series; HMB = High Magadi Beds). Green Beds radiometric dates are based on (1) Behr (2002) and this (2) paper.

Phosphate, which is released following weathering becomes available to plants, and is then concentrated in soils following decay of litterfall (Ruttenberg, 2014). Consequently, the elevated P_2O_5 could reflect P delivery to the palaeolake from soils enriched in P, implying a relatively wet climate. Dericquebourg et al. (2015), for example, suggested that phosphatic sediments in Miocene Lake Lukeino (central Kenya Rift) record high runoff to that palaeolake from organic-rich forest-covered soils. Ostracods and gastropods in the early Magadi palaeolake also indicate that it was then shallow and dilute. The absence of pollen, common in overlying sediments, implies oxic bottom waters, which would have favoured phosphorus deposition (Cosmidis et al., 2014).

Chert began to accumulate from about 1 Ma ago, implying that early north-south rift faulting might have provided pathways for silica-rich deep fluids to reach the surface (Owen et al., 2018b), supplementing the silica derived from chemical weathering and runoff. Later, intermittent development of chert implies continued inflow of silica-rich runoff, spring- and groundwaters, with periodic development of evaporative alkaline brines that underwent dilution, cooling or both, perhaps with microbial mediation of some silica precipitation.

Zone G3 (~740–545 ka) correlates with upper Stage D1, which lacks diatoms, perhaps reflecting dissolution, competitive exclusion or high turbidity. K + Na/Al ratios increase and P_2O_5 decreases in G3, with the sediments containing Mg-calcite and dolomite. Those minerals typically form in alkaline waters with high Mg/Ca ratios (Last et al., 2012), and imply lake- or pore-fluids with a Mg/Ca ratio high enough to induce primary carbonate precipitation or early diagenetic alteration of a carbonate precursor (Murphy et al., 2014).

REE data for G3 (Fig. 11) show similarities to G1–G2 indicating weathering of trachytic bedrock. However, relatively steep REE patterns, reflected in normalised La/Lu ratios, suggest an increase in basaltic bedrock sources. This inference is supported by increased Co, Cr, Cu, Ni and V, which are more abundant in rift basalt. The REE changes and increase in transition metals might have been induced by N-S axial-rift faulting that fragmented the basin and eroded trachyte, locally exposing older rocks. Potential sources include the Ol Tepesi, Singaraini and Kirikiti Basalts, and basalt along the rift margins or beyond (Baker, 1958; Guth and Wood, 2014). In all cases, cross-rift lateral drainage is implied for mafic siliciclastics to have reached the MAG14-2A site. Increased organic carbon and sulfur (Fig. 9), and development of euhedral pyrite crystals (~3 mm) in G3b upwards indicate increased bottom-water anoxia. Redox-sensitive trace-metals (Mo, Cd, U) also increase in G3, as they do today in the deeper, anoxic and sulfidic waters of Lake Tanganyika (Brucker et al., 2011).

Aquatic sedimentation during G4 times (~545–380 ka) appears to have been continuous at the MAG14-2A site despite outcrop distributions that indicate that the palaeolake had shrunk in size. This zone overlaps with stages D2, D3 and lower D4, in which diatoms are rare. Floras are dominated by planktonic species that include freshwater

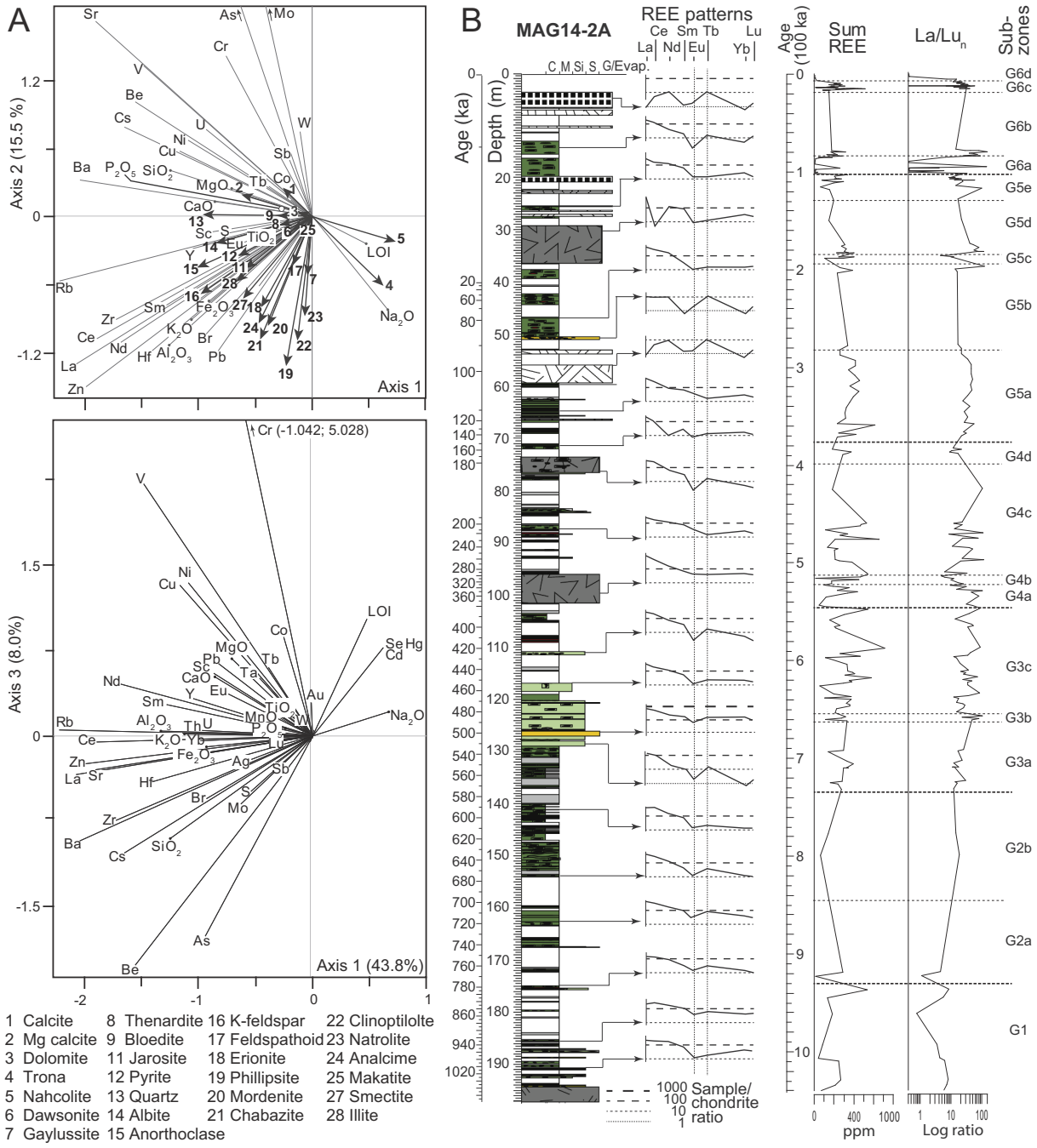

Fig. 11. Elemental relationships and REE variability. A: PCA analyses show a close relationship between REE, Al_2O_3, Fe_2O_3 and TiO_2, indicating that the REE (e.g., La, Ce, Sm, Eu) are probably detrital. Potential rift-valley sources include trachytes and basalts, with the former typically showing a negative Eu anomaly that is absent in basalts. B: Stratigraphic variability in REE versus core depth and time. Note the distinctive Eu anomalies below 140 m core depth, which closely resemble an unaltered trachyte REE pattern. From 140 to 100 m, REE patterns become more variable and La/Lu ratios increase. Above 100 m there is extreme variability in REE data with variable negative REE anomalies. This likely reflects complexation with carbonates in increasingly saline and alkaline waters. Geochemical zones noted to the right for comparison.

Aulacoseira mixed with saline *Cyclotella meneghiniana* and *Thalassiosira faurii* (Fig. 10), with mean transfer-functions implying pH of ~7.4–8.5 and conductivities of ~300–3000 μS cm^{-1}. Co decreases sharply at the base of G4, together with declining Cr, Cu, Ni and V (Fig. 9B), reflecting reduced basaltic inputs, perhaps due to (1) diminished weathered basaltic terrains, (2) increased aridity and (or) reduced fluvial flow from basaltic terrains, or (3) rising horst-blocks that deflected drainage axially, in common with regional N-S tilting (Owen et al., 2014).

Ca/Na and (K + Na)/Al ratios increase slightly in G4, with analcime common and rare natrolite, erionite and phillipsite, indicating higher salinity, consistent with increasing regional aridity (Fig. 9A). P_2O_5 remained low during G4 deposition with well-preserved organic matter and lamination implying an anoxic lake floor. Variable chondrite-normalised La/Lu ratios and Eu anomalies, first observed in G3, continue. G4 REE patterns show strongly negative Eu anomalies, declining LREE and flat to declining HREE, with variable total REE (Fig. 11B). The REE patterns resemble those for rocks of the Magadi Trachyte Formation (Owen et al., 2011), but with a distinctive depletion in Lu similar to

samples from Late Pleistocene spring tufa at Olorgesailie (Lee et al., 2013).

Zone G5 (~380–105 ka) coincides with upper D4 to lower D8, which contain rare to common, mixed saline and freshwater, planktonic diatoms dominated by *Aulacoseira*, *Thalassiosira* and *Cyclotella*. Episodic increases in freshwater benthic species (Fig. 10) may indicate dilute inflow during floods (Barker et al., 1990). One explanation for mixing of saline and freshwater floras could be that a saline alkaline lake was periodically, or seasonally, flooded by fresh, lower-density nutrient-rich waters and became meromictic, similar to modern Lake Bogoria (Fig. 12D; De Cort et al., 2018). Potential water sources include axial rivers and dilute overflow from the Koora Graben to the east. Diatoms could have lived in the fresh surface waters (mixolimnion) if essential nutrients remained available and evaporative concentration did not exceed their salinity tolerances.

Zone G5 is characterised by very low Ca/Na and low (K + Na)/Al ratios (Fig. 9A). Models of brine evolution reflect critical geochemical divides and pathways that help to explain the Magadi hydrochemistry (Hardie and Eugster, 1970; Deocampo and Jones, 2014). Today, Lake Magadi brines form following the evaporation of dilute inflow with $HCO_3 \gg Ca + Mg$. Early precipitation of calcite and Mg-calcite (plus minor primary or replacement dolomite?) in subsurface flow paths, at or near spring discharges, at the lake margin, or in the water column leads to a Ca- and Mg-free Na-CO_3-SO_4-Cl brine (Deocampo and Renaut, 2016). Microbial sulfate reduction then produces Na-CO_3-Cl fluids from which trona and halite precipitate (Hardie and Eugster, 1970; Jones et al., 1977; Eugster, 1986). Lower Ca content in G5 likely reflects these processes and (or) proportionally more hydrothermal inflow with low Ca and high Na, as is typical for most of the modern hot springs (Jones et al., 1977; Allen et al., 1989).

Zone G5 sediments contain many zeolites (natrolite, chabazite, erionite, phillipsite, clinoptilolite) but lack calcite or Mg-calcite, reflecting increasingly saline and alkaline waters (Rabideaux, 2018). Many zeolites formed during early diagenesis (cf. Hay, 1966, 1970; Manega and Bieda, 1987). Erionite, the most common zeolite, forms where trachytic glass reacts with water. Later zeolite phases formed where erionite or other precursors reacted with more concentrated brines (Herrick, 1972; Surdam and Eugster, 1976). Erionite + Na^+

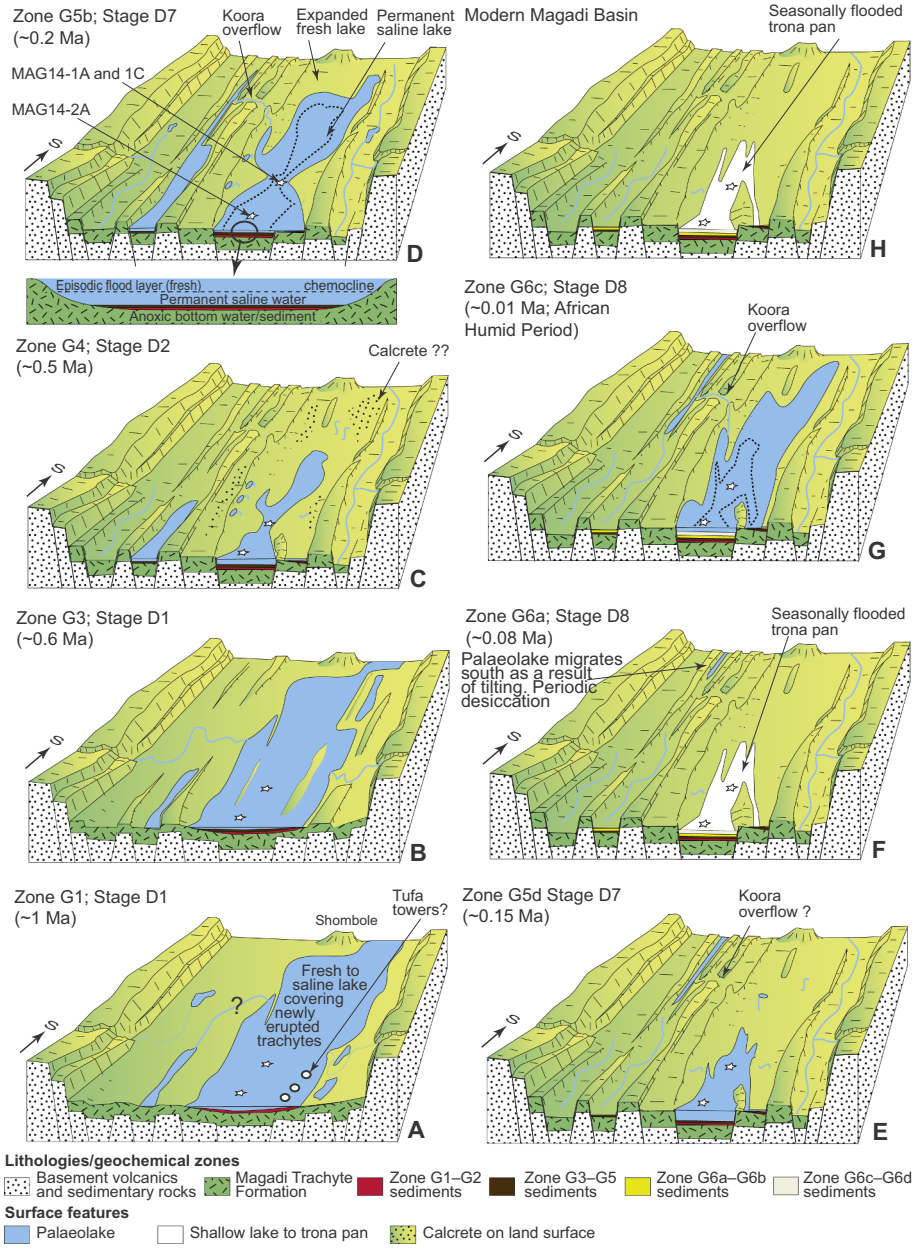

Fig. 12. Evolving palaeogeography of the Magadi Basin through time. Stars mark approximate position of core sites (labelled in 'D'). Box titles refer to geochemistry (G) and diatom (D) stages. A: Early (~1 Ma) development of broad, shallow, fresh to saline palaeolake. Subdued relief on Magadi Trachyte flood lavas. Subaqueous tufa towers develop in western areas? B: Faulting starts to break up the basin, but a moderately large saline lake remains. Basaltic weathering products linked to erosion of axial-rift-faulted Magadi Trachyte are supplemented by basalt eroding along rift margins. C: Continued axial-rift faulting causes further basin breakup. Lateral drainage diverted along grabens as axial-rift faulting increases, with reduced basaltic inputs to Lake Magadi. The palaeolake shrinks due to increasing aridity, with widespread calcrete formation across the semi-arid drainage basin. D: Formation of a periodically meromictic saline lake. Possible overflow from Koora Basin to the southeast? E: Expansion and contraction of a periodically meromictic, saline alkaline lake. F: Formation of seasonal playa lake similar to modern Lake Magadi. G: African Humid Period with expansion to form a meromictic, saline alkaline lake in which the High Magadi Beds accumulated. H: Modern Lake Magadi. Spring-fed trona pan flooded seasonally by axial rivers.

produces analcime and is favoured by high Na^+/H^+ ratios and low silica activity. In contrast, phillipsite forms by reaction of trachytic glass with Ca^+ and K^+ -bearing fluids associated with high silica activity. Herrick (1972) noted that analcime might form from aluminosilicate gels, which are often present in modern sediments at Nasikie Engida (Fig. 1A), a small hyperalkaline lake northwest of Lake Magadi (Eugster and Jones, 1968). Hay (1964) inferred that dominance of erionite over phillipsite reflects high Na/K ratios in brines, with phillipsite associated with ratios of 28–34. In contrast, chabazite requires more Ca to form (Singer and Stoffers, 1980), and clinoptilolite needs high silica activity (Herrick, 1972).

Zone G5 REE patterns vary more than those in G1–G4. Some show negative Eu anomalies, but others do not. Tb is lower in some G5 samples. Nd and Sm also change with HREE showing falling, flat and rising trends. Kerrich et al. (2002) reported REE variability in outcrops of the Green Beds and High Magadi Beds, which correlate with parts of G5 and G6, respectively (Fig. 9A). Although REE are commonly used in provenance studies because of their stability (Taylor and McLennan, 1985), they vary in response to changes in pH, redox conditions, adsorption/desorption and cation exchange in highly saline alkaline lakes. Lee and Byrne (1993), for example, noted that carbonate-rich brines have a significant impact on REE speciation and in complexing REEs.

Zone G6 (~105–0 ka) sediments, characterised by very low Ca/Na, high (K + Na)/Al ratios and high LOI_{550} percentages, include many zeolites, abundant trona and minor nahcolite (Fig. 9A). Stage D8 (120–16 ka, Fig. 10) overlaps with G6a–G6c, with diatoms declining in abundance upwards. Taxa include mixed freshwater *Aulacoseira* spp. and saline *Thalassiosira* and *Cyclotella* taxa. The mixed flora, similar to that in G5, implies periodic flooding and the formation of meromictic lakes of variable duration, with sparse floras after about 0.08 ka consistent with development of a trona saline pan.

REE data vary more than in lower zones (Fig. 11B). Detailed G6 REE patterns show that trona-bearing mud has a negative Eu anomaly and that REEs decline from LREE to HREE (Fig. 11) except for Lu, which shows both negative and positive anomalies. In contrast, trona shows positive anomalies for Nd and Tb with low La, Sm, Eu and Yb, and a small positive anomaly for Lu, probably reflecting the influence of strongly alkaline carbonate-rich brines.

Relatively high Au concentrations in G6c, which partially overlaps with the African Humid Period (AHP) and HMB deposition, contrast with Au concentrations below detection limits in G6a–G6b and G6d at times when the basin was a trona pan. Zone G6a has less As, Br, Sb and REE than G6b (Fig. 9B) with G6c distinguished from G6b by higher concentrations of Br, Ag, Pb, Th, U and Zn, together with less As, Mo and Sb. Several of these elements (Br, Pb, Zn, Sb, Ag) have been related to springs feeding carbonate lakes at Sassykkul in Tajikistan (Volkova, 1998). Other elements were considered tracers of evaporative concentration (U, Mo, As) at Sassykkul. Variations in these elements might reflect contrasting spring sources and brine evolution in palaeolake Magadi. Br shows very-low positive or negative correlations with other elements, with Br concentrations increasing and Ca/Na ratios decreasing upwards (Fig. 9B), which may indicate a link to increasing salinity and possible hydrothermal inflow.

5.1.2. Outcrop to core correlation and palaeogeography

Outcrop to core correlations are shown in Figs. 9, 10 and 13. The Magadi outcrop and core sediments lie upon the Magadi Trachyte Formation (~1.4–0.8 Ma), which consists of flood trachyte up to 120 m thick that filled the pre-existing horst-and-graben topography. Rivers and lakes then deposited fluvial and lacustrine sediments upon the volcanic substrate (Baker, 1958; Crossley and Knight, 1981; Guth and Wood, 2014).

The poorly dated Oloronga Beds began to accumulate before 0.78 ± 0.04 Ma based on a K-Ar date from obsidian within basal Oloronga lake beds (Fairhead et al., 1972; Eugster, 1980, his Fig. 15.21). A U/Th-dated hippo tooth gave a minimum age of 300 ka for the upper Oloronga Beds (Röhricht, 1998; Behr and Röhricht, 2000), although the actual ages of these beds could be much older. The lack of pedogenesis upon the trachyte substrate at MAG14-2A implies that deposition started soon after eruptions ceased (~1078.3 ± 3.6 ka). Together, the evidence from cores and the distribution of the Oloronga Beds, show that the earliest palaeolakes (Zones G1–G2, ~1056–740 ka) were fresh to mildly saline and more extensive than today (Fig. 12A).

Tufa-travertine towers on a horst west of Lake Magadi have been radiocarbon dated at 16.7 ± 0.4 to 25.5 ± 0.7 ka (Hillaire-Marcel et al., 1986) and were interpreted to have formed while partly submerged near the HMB palaeolake shoreline. However, they are possibly much older, given that the base of the largest tower (~712 m asl) is > 50 m higher than the maximum inferred Late Pleistocene-Holocene HMB lake-level (~660 m asl) (Hillaire-Marcel et al., 1986). It is unclear if the tufa deposits are subaerial or sublacustrine or both, but the towers lack external drapery that might be expected with subaerial outflow (cf. Bargar, 1978). Possible rimstone dams south of the towers imply subaerial formation and the dense travertine fabrics of those dams are compatible with high-temperature fluids (Jones and Renaut, 2010). In contrast, the towers, with internal vertical tubes, are similar to those described from lake floors (e.g., Lake Abhé: Dekov et al., 2014). A sublacustrine origin (Casanova and Hillaire-Marcel, 1987, their Fig. 9) would imply a Holocene lake at ~715–720 m or higher, for which there is no recorded evidence. Either the horst block has been uplifted > 50 m during the terminal Pleistocene and Holocene, or the tufa towers may be contemporary with the small Oloronga tufa chimneys at Section OB1, having formed before axial-rift faulting, and contemporary with Zone G1 (1080–930 ka) when carbonate grainstone was deposited (Fig. 12A). Baker (1958) found no evidence for tectonic disturbance of the HMB and recorded the '40 ft' (+12.2 m: ~617–620 m: Fig. 7A) shoreline at many locations across the basin. Behr (2002, p. 260) similarly found no sedimentary or geomorphological evidence for a higher precursor lake at that time. The age of the tufa towers remains uncertain.

The distribution of sediment outcrops that are contemporary with Zone G3 (~740–545 ka) suggests a similar areal extent for the Magadi palaeolake to that inferred for G1–G2 times (Fig. 12B). Faulting increased the topographic expression of north-south trending grabens, some of which might have hosted isolated or periodically interconnected lakes.

In outcrop, the Oloronga Beds are commonly capped by pisolitic to massive calcrete (Fig. 4A, D and E) that implies prolonged semi-aridity and relatively low lake level. In cores, the boundary between Zones G4 and G5 (Fig. 9A) is characterised by reduced Ca/Na ratios and a change from calcite and Mg-calcite to zeolites, which indicates an increase in palaeosalinity consistent with increased aridity at ~380 ka. The widespread calcrete overlies laterally extensive and eroded Oloronga Beds (Eugster, 1980; Felske, 2016) with younger outcrop sediments restricted to the modern axial lake basin, which suggests that the G4 (~545–380 ka) palaeolake had permanently shrunk (Fig. 12C), likely due to faulting and basin fragmentation that developed an axial horst-and-graben topography. Increased tectonic activity at Magadi during this interval is consistent with evidence from the Olorgesailie Basin, ~20 km to the northeast, where faulting disrupted that basin after ~500 ka (Behrensmeyer et al., 2018; Potts et al., 2018).

During G5 times (~380–105 ka), a saline, alkaline lake developed that might have been periodically flooded by axial rivers, or perhaps overflow from a contemporary lake in the neighbouring Koora Basin to the east (Fig. 12D–E) (Baker, 1958, 1986; Marsden, 1979; Muiruri, 2018). Although the timing of any overflow episodes is uncertain, evidence for such events are preserved in a deep NW-SE fault-controlled channel incised into Magadi Trachyte and by palaeowaterfalls to the southeast of modern Lake Magadi, near Karamai. Composite cores MAG14-1A and MAG14-1C (Fig. 12D), between the north and central Lake Magadi sub-basins, contain orthoconglomerate that correlates with G5. These gravels accumulated on a shallow E-W tectonic sill. In

contrast, MAG14-2A lies in the deeper north Magadi sub-basin and remained wet even during times of increased aridity, perhaps due to spring inflow.

The Green Beds, south and northeast of the modern lake, are contemporary with upper Zone G5 and possibly lower G6. They were previously dated at 98.5 ± 20 ka and 40.0 ± 6.5 ka using U/Th techniques (Goetz and Hillaire-Marcel, 1992). New U/Th dates from bedded cherts obtained for this study indicate ages of 180.6 ± 19.5, 176.6 ± 23.7, and 158.4 ± 17.4 ka. Chert dykes that intrude the Green Beds have ages of 191.8 ± 3.6, 166.9 ± 3.3 and 163.0 ± 3.3 ka. The latter dates might reflect initial chert formation rather than the age of dyke injection but all are older (~191–158 ka) than those proposed by Goetz and Hillaire-Marcel (1992) and Behr (2002). The revised chert ages correlate with zones G5c–d (Fig. 9B) and diatom stage D7 (Fig. 10). Outcrops of the Green Beds imply deposition on a gently sloping playa margin during the later stages of Zone G5 with upward-shallowing cycles, strong evaporation, and with microbialites and bedded chert forming periodically in shallow saline, alkaline waters.

Zone G6 is poorly represented in outcrops as it represents a time when Lake Magadi was generally low and confined to the axial graben as a small highly saline lake or trona pan (Fig. 12F). However, there were wetter intervals when the lake expanded as it did during the African Humid Period (Fig. 12G). Butzer et al. (1972), for example, reported a ^{14}C date of 9120 ± 120 yr BP for a fish-bearing clay marker-bed in the lower HMB (Figs. 6, 7D). They also reported "corrected" ^{14}C trona dates from a mid-basin core of 4600 (11 m depth), 5750 (21.4 m) and 10,010 (47.5 m) yr BP (errors unreported) in the Evaporite Series but questioned their reliability. Despite the age uncertainty, these deposits represent Holocene periods when the palaeolake resembled the modern evaporative lake (Fig. 12H). Williamson et al. (1993) also obtained U/Th dates from a core in the 'Northwest Arm' of Lake Magadi of

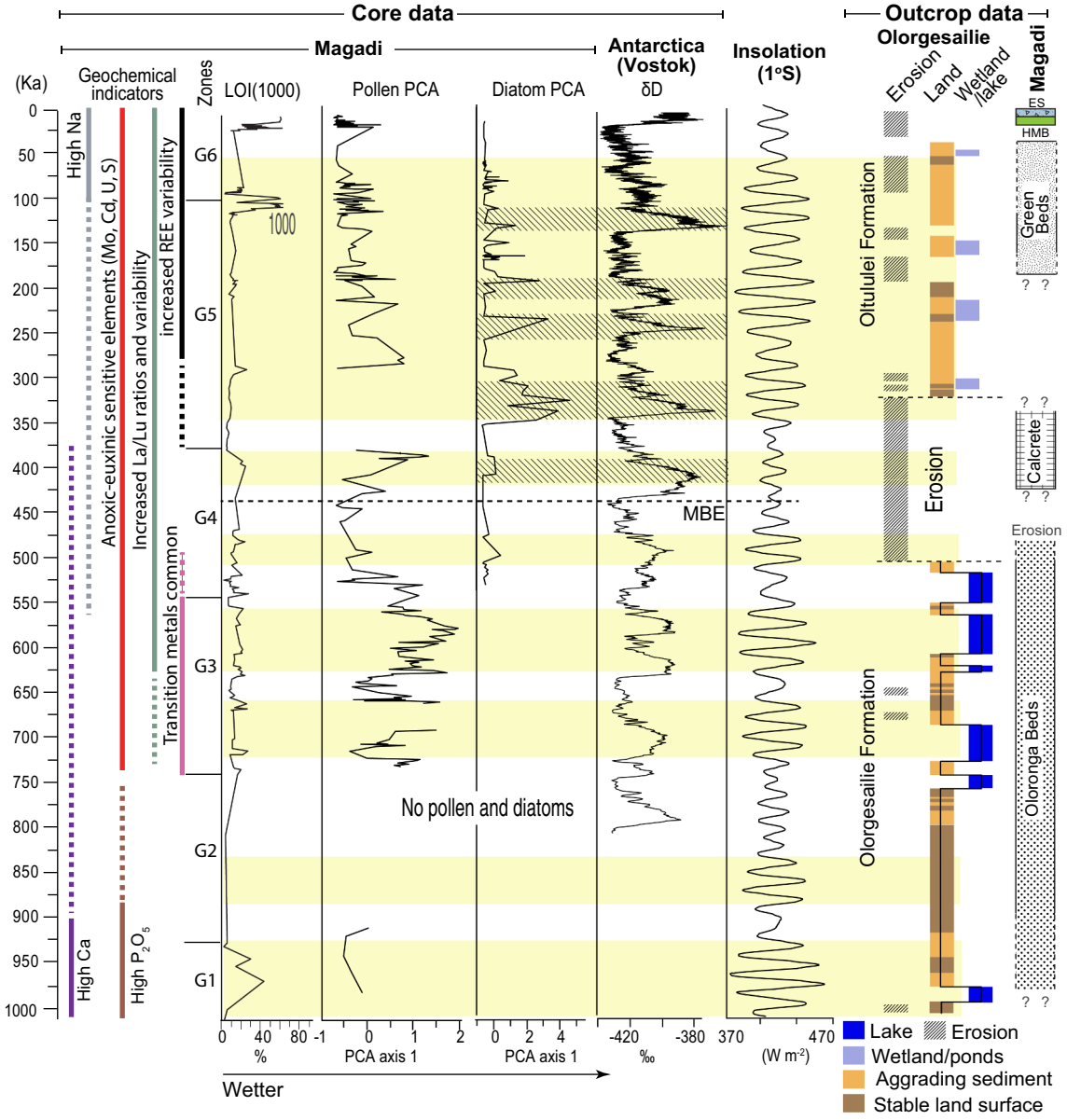

Fig. 13. Magadi Basin: regional and global comparisons. Magadi data compared with climate indicators from Jouzel et al. (2007) and Owen et al. (2018a). Yellow shading indicates periods of high variability insolation. Links to global climate patterns are shown. For example, diagonal patterns compare interglacials (Vostok data) with Magadi diatom PCA reflecting flooding episodes. Outcrop correlations shown to the right (ES = Evaporite Series; HMB = High Magadi Beds). Lake level fluctuations for Olorgesailie from Potts et al. (2018). See text for discussion. MBE = Mid-Brunhes Event. (For interpretation of the references to colour in this figure legend, the reader is referred to the web version of this article.)

40,000 ± 6500 and 23,700 ± 6000 yr BP with HMB high lake deposits dated at 12,090 ± 120 and 10,800 ± 120 yr BP. The HMB and Evaporite Series would therefore correlate with Zones G6c and d in MAG14-2A, and parts of Stage D9 (Figs. 9 and 10).

5.2. Controls on sedimentation

Sedimentation in the Magadi Basin was influenced by climate, tectonics and volcanism. The importance of climate is confirmed by pollen and diatom data, which record a drying trend after ~575 ka and many links to global climate trends (Owen et al., 2018a). For example, diagonal shading in Fig. 13 shows correlations between interglacials (Antarctica data: Jouzel et al., 2007) and influxes of benthic diatoms (high PCA values) that imply flooding of the palaeolake. Periods when conditions were wetter in the Magadi Basin (750–525 ka) were also recorded in the Olorgesailie Basin, 20 km to the northeast, as shown by correlations between high pollen PCA values (Fig. 13) and inferred high lake-levels (Potts et al., 2018). These reversible changes are unlikely to have been driven by uplift or subsidence, which tends to be directional in rift settings, especially on the timescales involved.

In contrast, the geochemical data (Figs. 9 and 13), discussed below, include episodes when abrupt step-like changes occurred that might reflect tectonic controls. For example, a major transition at ~740 ka led to an increase in anoxic-euxinic elements (Mo, Cd, U, S) in the sediments. LOI percentages also increased, pollen started to be well-preserved, La/Lu ratios became more variable and transition metals appeared in the geochemical record. A second step-like change occurred at ~ 105 ka ago with increased Na and the first appearance of trona in cores.

Owen et al. (2018b) documented several broad relationships between rifting and sedimentation across the East African Rift System, observing, for example, that axial subsidence can cause rainshadow effects which increase aridity on the rift floor. Fig. 14 shows major controls on Magadi basin sedimentation, emphasising the role of tectonics. The Magadi Rift was initiated at ~7 Ma (Foster et al., 1997; Lee et al., 2017). The oldest deposits are buried below the Magadi Trachytes (1.4–0.8 Ma). Early uplift along the rift margins would have cut off lateral drainage into the rift (Fig. 14A) restricting sediment supply,

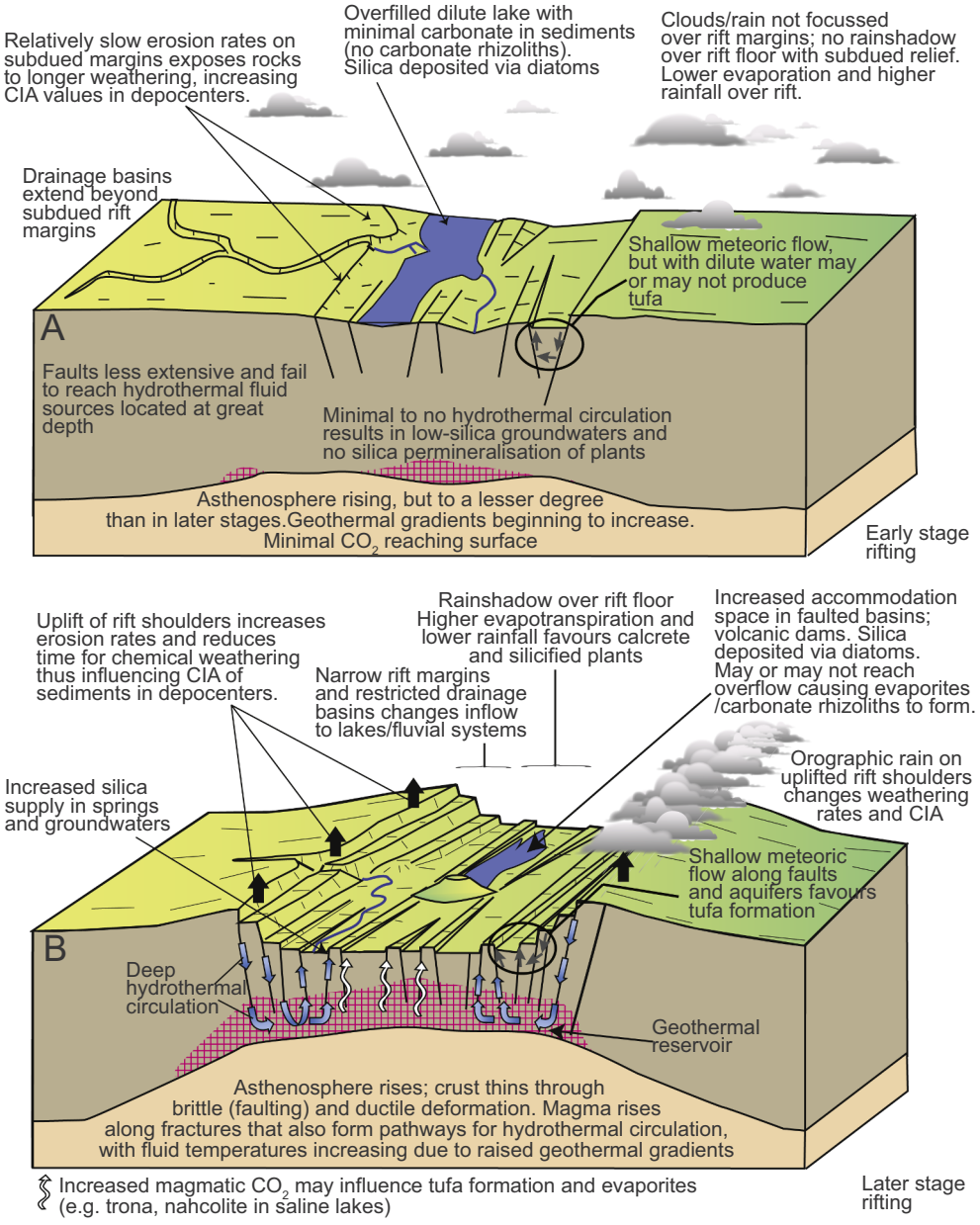

Fig. 14. Rifting and sedimentation. Major controls on sedimentation during early (A) and later (B) rifting, as at Magadi during the last 1 Ma. Modified from Owen et al. (2018b). Volcanic rocks commonly form dams providing hydrological closure. Uplift of rift margins and subsidence of the adjacent rift floor control orographic rainfall and development of rain shadows. Weathering and erosion are also influenced by uplift rates. CIA = Chemical Index of Alteration. Faulting controls accommodation space, outlet (sill) heights, drainage diversion, meteoric springs (A and B) and access to deep geothermal fluids (B). Geothermal fluids rise along faults, locally discharging at hot springs, augmenting silica supplied by weathering for chert formation. Trona-nahcolite evaporite precipitation is enhanced by addition of mantle CO_2.

reducing clastic input, and changing bedrock source lithologies and elemental compositions (solid and aqueous) delivered to the basin. Changes in subsidence and uplift would also have altered erosion, transportation and deposition rates that, in turn, would have controlled when rocks were exposed to weathering and its intensity.

Prior to the step-like change at ~740 ka, the volume of water inflow and sediment infill were broadly equal to the evolving accommodation (subsidence and compaction) in the rift grabens, producing 'balanced-filled' lakes (cf. Carroll and Bohacs, 1999). The earliest lakes were dilute to moderately saline, locally accumulating carbonate grainstone. After ~740 ka, the lakes became 'underfilled' when horsts and grabens fragmented the formerly flatter rift-floor. As axial-rift faulting proceeded and the climate became more arid, potential accommodation exceeded the volume of water and sediment supply. Closed hydrological basins then enabled the development of increasingly saline, alkaline lakes with anoxic bottom waters.

The presence of chert in the oldest Magadi sediments implies that early rising thermal fluids, and runoff with compositions derived from silicate weathering, contained enough silica for siliceous deposits to form after evaporation, evapotranspiration, dilution at a chemical interface, cooling or microbial biomediation. Crustal thinning above an elevated asthenosphere might have enabled faults to tap deep geothermal reservoirs (Fig. 14B) but subaerial sinter deposits, linked to boiling water, are rare in the south Kenya Rift. Palaeosinters (including fossil geyserite) are known only at Eremit ~15 km northeast of Olorgesailie (Owen et al., 2014). Most modern hydrothermal fluids at Magadi contain Na ≫ Ca and abundant HCO_3 and CO_3. These favour formation of Na-CO_3-SO_4-Cl brines with a high pH after evaporation (Eugster, 1970, 1980, 1986). Those fluids have exerted a major influence on deposition, especially since G5 times (after ~380 ka) when salinities increased and alkaline carbonate-rich fluids reacted with volcaniclastic particles to form zeolites. However, the contemporary alkaline water did not precipitate extensive trona until the second step-like change in the geochemical profile at about 105 ka ago.

That event might have involved a tectonic control. Earman et al. (2005), for example, emphasised the role of magmatic CO_2 in producing extensive deposits of trona in the USA and Mexico. Renaut and Tiercelin (1994) had earlier proposed that geothermal CO_2 contributed to trona formation at Lake Bogoria, Kenya. Gaseous CO_2 is trapped today below an extensive nahcolite ($NaHCO_3$) crust on the floor of Nasikie Engida, a small lake northwest of Lake Magadi (Fig. 1A). Darling et al. (1995) showed that abundant CO_2 of mantle origin is issues along the rift floor. Lee et al. (2016, 2017) reported that ~4 Mt yr^{-1} of mantle-derived CO_2 is released along faults in the Magadi–Natron Basin. It is possible, therefore, that formation of trona at Magadi was enhanced by CO_2-enriched gas discharge into the lake along sublacustrine faults, in addition to strong evaporation in an underfilled basin.

The origins of the Magadi chert deposits remain enigmatic (Eugster, 1967, 1969; Hay, 1968; Behr, 2002; Brenna, 2016; Leet et al., 2016). Eugster (1980) attributed the Magadi chert to replacement of magadiite [$NaSi_7O13(OH)_3.4H_2O$], other sodium silicates, or Na-silicate gels in the HMB sediments and at Nasikie Engida. In outcrop, most bedded chert in the Oloronga Beds and Green Beds are concordant within lacustrine sediments, whereas other cherts are intrusive, forming dykes, irregular masses and mounds (some biohermal?). Intrusions of silica-rich fluid, soft and semi-lithified silica gel, and chert into older shallow sediments are probably related to tectonic events (Behr and Röhricht, 2000). Some bedded chert in outcrop provides sedimentological evidence that implies microbial influences in its formation and shows that the quartz might originally have been soft gelatinous silica (Behr, 2002; Brenna, 2016). Evidence from the HSPDP cores implies several origins for the chert, but some chert horizons were clearly diagenetic (Leet et al., 2016). Behr (2002) reported that some exposed chert might have replaced carbonate. Rare examples of carbonate replacement by chert are exposed ~10 km SSE of Magadi townsite. High aqueous silica resulting from weathering (silicate hydrolysis of volcanic rocks), hydrothermal inflow, and highly alkaline (high pH) brines makes it difficult to differentiate the origins of the parent fluids and specific factors leading to silica precipitation (e.g., evaporation, fluid mixing, cooling and replacement of carbonate in various combinations). These processes nonetheless have produced what is perhaps the most extensive outcrop of lacustrine chert in the world.

6. Conclusions

The Magadi Basin preserves a one-million-year record of aquatic deposition under dry, tropical conditions. The basin experienced progressive increases in aridity superimposed on wet-dry cycles and step-like changes that resulted from tectonic processes. Major tectonic controls include:

- Axial rift faulting that tapped geothermal fluid reservoirs, introducing silica via springs from early in the basin history.
- Faulting of the rift floor that diverted cross-rift (E-W) rivers that reduced inputs of transition metals derived from rift-marginal basalts after 540 ka.
- The addition of magmatic CO_2 to evaporated sodic brines that enabled thick trona deposits to form after 105 ka.
- The development of a horst-and-graben topography that modified accommodation space and which confined the palaeolake to its present narrow N-S axial setting after deposition of the Oloronga Beds.

Climatically, the basin was characterised by many wet-dry cycles, but with a trend towards increasing aridity after 575 ka. This increased evaporative concentration of spring, stream and lake waters, resulting in:

- Higher pH and salinity. Mildly saline, calcite-precipitating, waters developed before 380 ka. Later high-pH waters reacted with volcaniclastic grains to form zeolites; trona precipitated after ~105 ka.
- Increased REE instability, with these elements complexing with carbonate as waters became more alkaline after 400 ka and especially after 105 ka.
- Saline lakes that received episodic fresh waters, leading to mixed assemblages of saline and freshwater planktonic diatoms between 545 and 16 ka.

The Quaternary sediments of the Magadi Basin record long-term climatic change (increasing aridity) and contemporary tectonics that frequently modified the hydrology and hydrogeology. The sedimentary record confirms the importance of considering all potential environmental controls when performing environmental reconstructions, especially in tectonically active settings.

Acknowledgements

Drilling was funded by ICDP and NSF grants (EAR-1123942, BCS-1241859, and EAR-1338553). Analyses were supported by the Hong Kong Research Grants Council (HKBU-201912 and 12304018). We thank the National Museums of Kenya, the Kenyan National Council for Science and Technology, the Kenyan Ministry of Mines, and the National Environmental Management Authority of Kenya for providing permits. We also thank DOSECC Exploration Services for drilling supervision, the Operational Support Group of ICDP for downhole logging and the US National Lacustrine Core Facility. Tata Chemicals Magadi Limited and the Magadi Administrative District of Kajiado County provided local support. Research was undertaken with support of the local Maasai community. The late Jean-Jacques Tiercelin, with John Ego (NOCK) and George Muia, helped to log outcrops. Luis Buatois provided help with description of the ichnofossils. This is publication # 18 of the Hominin Sites and Paleolakes Drilling Project.

Appendix A. Supplementary data

Geochemical and diatom data in Tables S1 and S2. Supplementary data to this article can be found online at https://doi.org/10.1016/j.palaeo.2019.01.017.

References

Allen, D.J., Darling, W.G., Burgess, W.G., 1989. Geothermics and hydrogeology of the southern part of the Kenya Rift Valley with emphasis on the Magadi-Nakuru area. In: British Geological Survey Research Report SD/89/1, (68 pp and appendices).

Anonymous, 1923. The soda deposits of Lake Magadi in Kenya. Bull. Imp. Inst. 21, 431–444.

Baker, B.H., 1958. Geology of the Magadi area. Geol. Surv. Kenya Rep. 42.

Baker, B.H., 1963. Geology of the area south of Magadi. Geol. Surv. Kenya Rep. 61.

Baker, B.H., 1986. Tectonics and volcanism of the southern Kenya Rift Valley and its influence on rift sedimentation. In: Frostick, L.E., Renaut, R.W., Reid, I., Tiercelin, J.-J. (Eds.), Sedimentation in the African Rifts. Geological Society, London, Special Publication 25, pp. 45–57.

Bargar, K.E., 1978. Geology and thermal history of Mammoth Hot Springs, Yellowstone National Park, Wyoming. In: U.S. Geological Survey Bulletin 1444.

Barker, P., Gasse, F., Roberts, N., Taieb, M., 1990. Taphonomy and diagenesis in diatom assemblages; a Late Pleistocene palaeoecological study from Lake Magadi, Kenya. Hydrobiologia 214, 267–272.

Behr, H.-J., 2002. Magadiite and Magadi-chert: a critical analysis of the silica sediments in the Lake Magadi Basin, Kenya. In: Renaut, R.W., Ashley, G.M. (Eds.), Sedimentation in Continental Rifts. SEPM Special Publication 73, pp. 257–273.

Behr, H.J., Röhricht, C., 2000. Record of seismotectonic events in siliceous cyanobacterial sediments (Magadi cherts), Lake Magadi, Kenya. Int. J. Earth Sci. 89, 268–283.

Behrensmeyer, A.K., Potts, R., Deino, A., 2018. The Oltulelei Formation of the southern Kenyan Rift Valley: A chronicle of rapid landscape transformation over the last 500 k.y. Geol. Soc. Am. Bull. 130, 1474–1492.

Blaauw, M., Christen, A., 2011. Flexible paleoclimate age-depth models using an autoregressive gamma process. Bayesian Anal. 6, 1–18.

Brenna, B.L., 2016. The Chemical, Physical, and Microbial Origins of Pleistocene Cherts at Lake Magadi, Kenya Rift Valley. MSc thesis. University of Saskatchewan.

Brucker, R.P., McManus, J., Severmann, S., Owens, J., Lyons, T.W., 2011. Trace metal enrichments in Lake Tanganyika sediments: Controls on trace metal burial in lacustrine systems. Geochim. Cosmochim. Acta 75, 483–499.

Butzer, K.W., Isaac, G.L., Richardson, J.L., Washbourn-Kamau, C., 1972. Radiocarbon dating of East African lake levels. Science 175, 1069–1076.

Campisano, C.J., Cohen, A.S., Arrowsmith, J.R., Asrat, A., Behrensmeyer, A.K., Brown, E.T., Deino, A.L., Deocampo, D.M., Feibel, C.S., Kingston, J.D., Lamb, H.F., Lowenstein, T.K., Noren, A., Olago, D.O., Owen, R.B., Pelletier, J.D., Potts, R., Reed, K.E., Renaut, R.W., Russell, J.M., Russell, J.L., Schäbitz, F., Stone, J.R., Trauth, M.H., Wynn, J.G., 2017. The Hominin Sites and Paleolakes Drilling Project: acquiring high-resolution paleoclimate records from the East African Rift System and their implications for understanding the environmental context of hominin evolution. PaleoAnthropology 2017, 1–43. https://doi.org/10.4207/PA.2017.ART104.

Carroll, A.R., Bohacs, K.M., 1999. Stratigraphic classification of ancient lakes: Balancing tectonic and climatic controls. Geology 27, 99–102.

Casanova, J., 1987. Stromatolites et hauts niveaux lacustres Pléistocènes du basin Natron-Magadi (Tanzanie-Kenya). Sci. Géol. Bull. 40, 135–153.

Casanova, J., Hillaire-Marcel, C., 1987. Chronologie et paléohydrologie des hauts niveaux quaternaires du basin Natron-Magadi (Tanzanie-Kenya) d'après la composition isotopique (^{18}O, ^{13}C, ^{14}C, U/Th) des stromatolites littoraux. Sci. Géol. Bull. 40, 121–134.

Cohen, A., Campisano, C., Arrowsmith, R., Asrat, A., Behrensmeyer, A.K., Deino, A., Feibel, Hill, A., Johnson, R., Kingston, J., Lamb, H., Lowenstein, T., Noren, A., Olago, D., Owen, R.B., Potts, R., Reed, K., Renaut, R., Schäbitz, F., Tiercelin, J.-J., Trauth, M., Wynn, J., Ivory, S., Brady, C., O'Grady, R., Rodysill, J., Githiri, J., Russell, J., Foerster, V., Dommain, R., Rucina, S., Deocampo, D., Billingsley, A., Beck, C., Dullo, L., Feary, D., Garello, D., Johnson, T., Junginger, A., Karanja, M., Kimburi, E., Mbuthia, A., McCartney, T., McNulty, E., Muiruri, V., Nambiro, E., Njagi, D., Norman, J., Rabideaux, N., Raub, T., Sier, M., Smith, P., Urban, J., Warren, M., Wondiymu, E., Yost, C., 2016. The hominin sites and paleolakes drilling project: inferring the environmental context of human evolution from Eastern African rift lake deposits. Sci. Drill. 21, 1–16.

Cosmidis, J., Benzerara, K., Morin, G., Busigny, V., Lebeau, O., Jézéquel, D., Noël, V., Dublet, G., Othmane, G., 2014. Biomineralization of iron-phosphates in the water column of Lake Pavin (Massif Central, France). Geochim. Cosmochim. Acta 126, 78–96.

Crossley, R., 1979. The Cenozoic stratigraphy and structure of the western part of the rift valley in southern Kenya. J. Geol. Soc. Lond. 136, 393–405.

Crossley, R., Knight, R., 1981. Volcanism in the western part of the rift valley in southern Kenya. Bull. Volcanol. 44, 117–128.

Damnati, B., Taieb, M., 1995. Solar and ENSO signatures in laminated deposits from Lake Magadi (Kenya) during the Pleistocene/Holocene transition. J. Afr. Earth Sci. 21, 373–382.

Damnati, B., Taieb, M., Williamson, D., 1992. Laminated deposits from Lake Magadi; climatic contrast during the maximum wet period 12,000–10,000 BP. Bull. Soc. Geol. Fr. 163, 407–414.

Damnati, B., Icole, M., Taieb, M., 2007. The application of organic carbon and carbonate stratigraphy to the reconstruction of lacustrine palaeoenvironments from Lake Magadi, Kenya. In: Runge, J. (Ed.), Dynamics of Forest Ecosystems in Central Africa during the Holocene: Past, Present, Future. Taylor and Francis, London, pp. 155–168.

Darling, W.G., 2001. Magadi and Suguta: The contrasting hydrogeochemistry of two soda lake areas in the Kenya Rift Valley. In: Cidu, R. (Ed.), Proceedings of the Tenth International Symposium on Water-Rock Interaction, WRI-10, Villasimius, Italy 10–15 July 2001. A.A. Balkema, Lisse, pp. 95–98.

Darling, W.G., Griesshaber, E., Andrews, J.N., Armannsson, H., O'Nions, R.K., 1995. The origin of hydrothermal and other gases in the Kenya Rift Valley. Geochim. Cosmochim. Acta 59, 2501–2512.

De Cort, G., Bessems, I., Keppens, E., Mees, F., Cumming, B., Verschuren, D., 2013. Late-Holocene and recent hydroclimatic variability in the Central Kenya Rift Valley: the sediment record of hypersaline lakes Bogoria, Nakuru and Elementeita. Palaeogeogr. Palaeoclimatol. Palaeoecol. 388, 69–80.

De Cort, G., Verschuren, D., Ryken, E., Wolff, C., Renaut, R.W., Creutz, M., Van der Meeren, T., Haug, G., Olago, D.O., Mees, F., 2018. Multi-basin depositional framework for moisture-balance reconstruction during the last 1300 years at Lake Bogoria, Central Kenya Rift Valley. Sedimentology 65, 1667–1696.

Dekov, V.M., Egue, N.M., Kamenov, G.D., Bayon, G., Lalonde, S.V., Schmidt, M., Liebetrau, V., Munnik, F., Fouquet, Y., Tanimizu, M., Awaleh, M.O., Guirreh, I., Le Gall, B., 2014. Hydrothermal carbonate chimneys from a continental rift (Afar Rift): Mineralogy, geochemistry, and mode of formation. Chem. Geol. 387, 87–100.

deMenocal, P., 1995. Plio-Pleistocene African climate. Science 270, 53–59.

deMenocal, P., 2004. African climate change and faunal evolution during the Pliocene-Pleistocene. Earth Planet. Sci. Lett. 220, 3–24.

Deocampo, D.M., Jones, B.F., 2014. Geochemistry of saline lakes. In: Holland, H.D., Turekian, K.K. (Eds.), Treatise on Geochemistry, Second edition. vol. 7. Elsevier, Oxford, pp. 437–469.

Deocampo, D.M., Renaut, R.W., 2016. Geochemistry of African soda lakes. In: Schagerl, M. (Ed.), Soda Lakes of East Africa. Springer, Switzerland, pp. 77–96.

Dericquebourg, P., Person, A., Ségalen, L., Pickford, M., Senut, B., Fagel, N., 2015. Environmental significance of Upper Miocene phosphorites at hominid sites in the Lukeino Formation (Tugen Hills, Kenya). Sediment. Geol. 327, 43–54.

Earman, S., Phillips, F.M., McPherson, B.J.O.L., 2005. The role of "excess" CO_2 in the formation of trona deposits. Appl. Geochem. 20, 2217–2232.

Eugster, H.P., 1967. Hydrous sodium silicates from Lake Magadi, Kenya: precursors of bedded chert. Science 157, 1177–1180.

Eugster, H.P., 1969. Inorganic bedded cherts from the Magadi area, Kenya. Contrib. Mineral. Petrol. 22, 1–31.

Eugster, H.P., 1970. Chemistry and origin of the brines of Lake Magadi, Kenya. In: Mineralogical Society of America Special Publication 3, pp. 215–235.

Eugster, H.P., 1980. Lake Magadi, Kenya and its precursors. In: Nissenbaum, A. (Ed.), Hypersaline Brines and Evaporites. Elsevier, Amsterdam, pp. 195–232.

Eugster, H.P., 1986. Lake Magadi, Kenya: a model for rift valley hydrochemistry and sedimentation. In: Frostick, L.E., Renaut, R.W., Reid, I., Tiercelin, J.-J. (Eds.), Sedimentation in the African Rifts. Geological Society of London Special Publication 25, pp. 177–189.

Eugster, H.P., Hardie, L.A., 1978. Saline lakes. In: Lerman, A. (Ed.), Lakes: Chemistry, Geology, Physics. Springer-Verlag, Berlin, pp. 237–293.

Eugster, H., Jones, B., 1968. Gels composed of sodium-aluminum silicate, Lake Magadi, Kenya. Science 161, 160–163.

Eugster, H.P., Jones, B.F., 1979. Behavior of major solutes during closed-basin brine evolution. Am. J. Sci. 279, 609–631.

Fairhead, J., Mitchell, J., Williams, L., 1972. New K/Ar determinations on rift volcanics of S. Kenya and their bearing on age of rift faulting. Nature 238, 66–69.

Felske, G.N., 2016. Genesis of Calcretes and Related Carbonate Rocks in the Southern Kenya Rift. MSc thesis. University of Saskatchewan.

Foster, A., Ebinger, C., Mbede, E., Rex, D., 1997. Tectonic development of the northern Tanzanian sector of the East African Rift System. J. Geol. Soc. Lond. 154, 689–700.

Goetz, C., Hillaire-Marcel, C., 1992. U-series disequilibria in early diagenetic minerals from Lake Magadi sediments: dating potential. Geochim. Cosmochim. Acta 56, 1331–1341.

Gregory, J.W., 1921. The Rift Valleys and Geology of East Africa. Seeley Service, London.

Guth, A., Wood, J., 2014. Geology of the Magadi area. Geological Society of America, Digital Map and Chart Series, DMCH016.

Hardie, L.A., Eugster, H.P., 1970. The evolution of closed-basin brines. In: Mineralogical Society of America Special Publication 3, pp. 273–290.

Hay, R.L., 1964. Phillipsite of saline lakes and soils. Am. Mineral. 49, 1366–1387.

Hay, R.L., 1966. Zeolites and zeolitic reactions in sedimentary rocks. In: Geological Society of America Special Paper 85.

Hay, R., 1968. Chert and its sodium-silicate precursors in sodium-carbonate lakes of East Africa. Contrib. Mineral. Petrol. 17, 255–274.

Hay, R.L., 1970. Silicate reactions in three lithofacies of a semi-arid basin, Olduvai Gorge, Tanzania. In: Mineralogical Society of America Special Publication 3, pp. 237–255.

Herrick, R., 1972. Authigenic Minerals in the Pleistocene and Recent Sediments of Lake Magadi, Kenya. MSc thesis. University of Wyoming.

Hillaire-Marcel, C., Casanova, J., 1987. Isotopic hydrology and paleohydrology of the Magadi (Kenya)-Natron (Tanzania) Basin during the late Quaternary. Palaeogeogr. Palaeoclimatol. Palaeoecol. 58, 155–181.

Hillaire-Marcel, C., Carro, O., Casanova, J., 1986. ^{14}C and Th/U dating of Pleistocene and Holocene stromatolites from East African palaeolakes. Quat. Res. 25, 312–329.

Ivory, S.J., Blome, M.W., King, J.W., McGlue, M.M., Cole, J.E., Cohen, A.S., 2016. Environmental change explains cichlid adaptive radiation at Lake Malawi over the past 1.2 million years. Proc. Natl. Acad. Sci. 113, 11895–11900.

Jones, B., Renaut, R.W., 2010. Calcareous spring deposits in continental settings. In: Alonzo-Zarza, A.M., Tanner, L.H. (Eds.), Carbonates in Continental Settings: Facies, Environments, and Processes (Developments in Sedimentology 61). Elsevier,

Amsterdam, pp. 177–224.
Jones, B.J., Rettig, S.L., Eugster, H.P., 1967. Silica in alkaline brines. Science 158, 1310–1314.
Jones, B.J., Eugster, H.P., Rettig, S.F., 1977. Hydrochemistry of the Lake Magadi basin, Kenya. Geochim. Cosmochim. Acta 41, 53–72.
Jouzel, J., Masson-Delmotte, V., Cattani, O., Dreyfus, G., Falourd, S., Hoffmann, G., Minster, B., Nouet, J., Barnola, J.M., Chappellaz, J., Fischer, H., Gallet, J.C., Johnsen, S., Leuenberger, M., Loulergue, L., Luethi, D., Oerter, H., Parrenin, F., Raisbeck, G., Raynaud, D., Schilt, A., Schwander, J., Selmo, E., Souchez, R., Spahni, R., Stauffer, B., Steffensen, J.P., Stenni, B., Stocker, T.F., Tison, J.L., Werner, M., Wolff, E.W., 2007. Orbital and millennial Antarctic climate variability over the past 800,000 years. Science 317, 793–796.
Junginger, A., Trauth, M.H., 2013. Hydrological constraints of paleo-Lake Suguta in the Northern Kenya Rift during the African Humid Period (15–5 ka BP). Glob. Planet. Chang. 111, 174–188.
Kaufman, A., Margaritz, M.P.M., Hillaire-Marcel, C., Hollos, G., Boaretto, E., Taieb, M., 1990. The ^{36}Cl ages of the brines in the Magadi-Natron Basin, East Africa. Geochim. Cosmochim. Acta 54, 2827–2833.
Kerrich, R., Renaut, R.W., Bonli, T., 2002. Trace-element composition of cherts from alkaline lakes in the East African Rift: a probe for ancient counterparts. In: Renaut, R.W., Ashley, G.M. (Eds.), Sedimentation in Continental Rifts. SEPM Special Publication 73, pp. 275–294.
Kingston, J., Deino, A., Edgar, R., Hill, A., 2007. Astronomically forced climate change in the Kenyan Rift Valley 2.7–2.55 Ma: implications for the evolution of early hominin ecosystems. J. Hum. Evol. 20, 487–503.
Last, F.M., Last, W.M., Halden, N.M., 2012. Modern and late Holocene dolomite formation: Manito Lake, Saskatchewan, Canada. Sediment. Geol. 281, 222–237.
Le Roex, A.P., Späth, A., Zartman, R.E., 2001. Lithospheric thickness beneath the southern Kenya Rift: implications from basalt geochemistry. Contrib. Mineral. Petrol. 142, 89–106.
Lee, J.H., Byrne, R.H., 1993. Complexation of the trivalent rare earth elements (Ce, Eu, Gd, Tb, Yb) by carbonate ions. Geochim. Cosmochim. Acta 57, 295–302.
Lee, R.K.L., Owen, R.B., Renaut, R.W., Behrensmeyer, A.K., Potts, R., Sharp, W.D., 2013. Facies, geochemistry and diatoms of late Pleistocene Olorgesailie tufas, southern Kenya Rift. Palaeogeogr. Palaeoclimatol. Palaeoecol. 374, 197–217.
Lee, H., Muirhead, J.D., Fischer, T.P., Ebinger, C.J., Kattenhorn, Sharp, Z.D., Kianji, G., 2016. Massive and prolonged deep carbon emissions associated with continental rifting. Nat. Geosci. 9, 145–149.
Lee, H., Fischer, T.P., Muirhead, J.D., Ebinger, C.J., Kattenhorn, S.A., Sharp, Z.D., Kianji, G., Takahata, N., Sano, Y., 2017. Incipient rifting accompanied by the release of subcontinental lithospheric mantle volatiles in the Magadi and Natron basin, East Africa. J. Volcanol. Geotherm. Res. 346, 118–133.
Leet, K., Lowenstein, T., Owen, R.B., Renaut, R., Deocampo, D., Cohen, A., McNulty, E., Muiruri, V., Rabideaux, N.M., Billingsley, A.L., Mbuthia, A., 2016. Origins of Magadi-type chert: New clues from the HSPDP Lake Magadi drill cores. In: Geological Society of America Abstracts with Program 48 (7), Paper 42–9.
Levin, N.E., 2015. Environment and climate of early human evolution. Annu. Rev. Earth Planet. Sci. 43, 405–429.
Magill, C.R., Ashley, G.M., Freeman, K.H., 2013. Ecosystem variability and early human habitats in eastern Africa. Proc. Natl. Acad. Sci. 110, 1167–1174.
Manega, P.C., Bieda, S., 1987. Modern sediments of Lake Natron, Tanzania. Sci. Géol. Bull. 40, 83–96.
Marsden, M., 1979. Origin and Evolution of the Pleistocene Olorgesailie Lake Series, Kenya Rift Valley. PhD thesis. McGill University, Canada.
Muiruri, V., 2018. Late Quaternary diatom and palynomorph stratigraphies and palaeoenvironments of the Koora Graben and Lake Magadi Basin, Kenya Rift Valley. PhD thesis. Hong Kong Baptist University.
Murphy, J.T., Lowenstein, T.K., Pietras, J.T., 2014. Preservation of primary lake signatures in alkaline earth carbonates of the Eocene Green River Wilkins Peak-Laney Member transition zone. Sediment. Geol. 314, 75–91.
Ng'ang'a, P., Muchane, M.W., Johnson, T.C., Sturgeon, K., 1998. Comparison of isotopic records in abiogenic and biogenic calcite from Lake Turkana, Kenya. In: Lehman, J.T. (Ed.), Environmental Change and Response in East African Lakes. Monographiae Biologicae 79, pp. 173–190.
Owen, R.B., Potts, R., Behrensmeyer, A.K., Ditchfield, P., 2008. Diatomaceous sediments and environmental change in the Pleistocene Olorgesailie Formation, southern Kenya Rift Valley. Palaeogeogr. Palaeoclimatol. Palaeoecol. 269, 17–37.
Owen, R.B., Renaut, R.W., Potts, R., Behrensmeyer, A.K., 2011. Geochemical trends through time and lateral variability of diatom floras in the Pleistocene Olorgesailie Formation, southern Kenya Rift Valley. Quat. Res. 76, 167–179.
Owen, R.B., Renaut, R.W., Behrensmeyer, A.K., Potts, R., 2014. Quaternary geochemical stratigraphy of the Kedong–Olorgesailie section of the southern Kenya Rift valley. Palaeogeogr. Palaeoclimatol. Palaeoecol. 396, 194–212.
Owen, R.B., Muiruri, V.M., Lowenstein, T.K., Renaut, R.W., Rabideaux, N., Luo, S., Deino, A.L., Sier, M.J., Dupont-Nivet, G., McNulty, E.P., Leet, K., Cohen, A.S., Campisano, C., Deocampo, D., Shen, C.-C., Billingsley, A., Mbuthia, A., 2018a. Progressive aridification in East Africa over the last half million years and implications for human evolution. Proc. Natl. Acad. Sci. 115 (44), 11174–11179. www.pnas.org/cgi/doi/10.1073/pnas.1801357115.
Owen, R.B., Renaut, R.W., Lowenstein, T.K., 2018b. Spatial and temporal geochemical variability in lacustrine sedimentation in the East African Rift System: evidence from the Kenya Rift and regional analyses. Sedimentology 65, 1697–1730.
Parkinson, J., 1914. The East African Trough in the neighbourhood of the soda lakes. Geogr. J. 44, 33–46.
Potts, R., Shipman, P., Ingall, E., 1988. Taphonomy, paleoecology, and hominids of Lainyamok, Kenya. J. Hum. Evol. 17, 597–614.
Potts, R., Behrensmeyer, A.K., Faith, J.T., Tryon, C.A., Brooks, A.S., Yellen, J.E., Deino, A.L., Kinyanjui, R., Clark, J.B., Haradon, C., Levin, N.E., Meijer, H.J.M., Veatch, E.G., Owen, R.B., Renaut, R.W., 2018. Environmental dynamics during the onset of the Middle Stone Age in eastern Africa. Science 360, 86–90.
Rabideaux, N., 2018. Late Quaternary East African Environmental Change Based on Mineralogical and Geochemical Analysis of Outcrop and Core Material From the Southern Kenya Rift. PhD thesis. Georgia State University.
Renaut, R.W., Tiercelin, J.-J., 1994. Lake Bogoria, Kenya Rift Valley: A sedimentological overview. In: Renaut, R.W., Last, W.M. (Eds.), Sedimentology and Geochemistry of Modern and Ancient Saline Lakes. SEPM Special Publication 50, pp. 101–123.
Roberts, N., Taieb, M., Barker, P., Damnati, B., Icole, M., Williamson, D., 1993. Timing of the Younger Dryas event in East Africa from lake-level changes. Nature 366, 146–148.
Röhricht, C., 1998. Lithologie und der Chertserien des Magadi Beckens, Lake Magadi, Kenia. PhD thesis. University of Göttingen.
Ruttenberg, K.C., 2014. The global phosphorus cycle. In: Holland, H.D., Turekian, K.K. (Eds.), Treatise on Geochemistry, Volume 10 (Biogeochemistry). Elsevier, pp. 499–558.
Scott, J.J., 2010. Saline Lake Ichnology: Composition and Distribution of Cenozoic Traces in the Saline, Alkaline Lakes of the Kenya Rift and Eocene Green River Formation. U.S.A. PhD thesis. University of Saskatchewan.
Shipman, P., Potts, R., Pickford, M., 1983. Lainyamok, a new middle Pleistocene hominid site. Nature 306, 365–368.
Singer, A., Stoffers, P., 1980. Clay mineral diagenesis in two East African lake sediments. Clay Miner. 15, 291–307.
Stone, J.R., Westover, K.S., Cohen, A.S., 2011. Late Pleistocene paleohydrography and diatom paleoecology of the central basin of Lake Malawi, Africa. Palaeogeogr. Palaeoclimatol. Palaeoecol. 303, 51–70.
Sun, S.-S., McDonough, W.F., 1989. Chemical and isotopic systematics of oceanic basalts: Implications for mantle composition and processes. In: Saunders, A.D., Norry, M.J. (Eds.), Magmatism in Ocean Basins. Geological Society of London, Special Publication 8, pp. 313–345.
Surdam, R.C., Eugster, H.P., 1976. Mineral reactions in the sedimentary deposits of the Lake Magadi region, Kenya. Geol. Soc. Am. Bull. 87, 1739–1752.
Taieb, M., Barker, P., Bonnefille, R., Damnati, B., Gasse, F., Goetz, C., Hillaire, C., Icole, M., Masault, M., Roberts, N., Vincens, A., Williamson, D., 1991. Histoire paléohydrologique du lac Magadi (Kenya) au Pleistocène superieur. C. R. Acad. Sci. II 313, 339–346.
Taylor, S.R., McLennan, S.H., 1985. The Continental Crust: its Composition and Evolution. Blackwell, Oxford.
Tierney, J.E., Russell, J.M., Huang, Y., 2010. A molecular perspective on Late Quaternary climate and vegetation change in the Lake Tanganyika basin, East Africa. Quat. Sci. Rev. 29, 787–800.
Verschuren, D., Chapman, D., 2008. Latitudinal linkages in late-Holocene moisture-balance variation. In: Battarbee, R.W., Binney, H.A. (Eds.), Natural Climate Variability and Global Warming. Wiley-Blackwell, Chichester, UK, pp. 189–231.
Volkova, N.I., 1998. Geochemistry of rare elements in waters and sediments of alkaline lakes in the Sassykkul depression, East Pamirs. Chem. Geol. 147, 265–277.
Walter, P., 1922. Sodium carbonate minerals of the Mogadi lakes, British East Africa. Am. Mineral. 7, 86–88.
White, T.H., 1953. Some speculations on the sudden occurrence of floods in the history of Lake Magadi. J. East Afr. Nat. Hist. Soc. 22, 69–71.
Williamson, D., Taieb, M., Damnati, B., Icole, M., Thouveny, N., 1993. Equatorial extension of the Younger Dryas event: rock magnetic evidence from Lake Magadi (Kenya). Glob. Planet. Chang. 7, 235–242.